Bioorganic Chemistry 110 (2021) 104765

Contents lists available at ScienceDirect

Bioorganic Chemistry

journal homepage: www.elsevier.com/locate/bioorg

Cinnamide derived pyrimidine-benzimidazole hybrids as tubulin inhibitors: Synthesis, *in silico* and cell growth inhibition studies

Sravani Sana [a], Velma Ganga Reddy [c,*], T. Srinivasa Reddy [c], Ramya Tokala [a], Rahul Kumar [b], Suresh K. Bhargava [c], Nagula Shankaraiah [a,*]

[a] Department of Medicinal Chemistry, National Institute of Pharmaceutical Education and Research (NIPER), Hyderabad 500 037, India
[b] Department of Pharmacology and Toxicology, National Institute of Pharmaceutical Education and Research (NIPER), Hyderabad 500 037, India
[c] Centre for Advanced Materials & Industrial Chemistry (CAMIC), School of Science, RMIT University, GPO Box 2476, Melbourne 3001, Australia

ARTICLE INFO

Keywords:
Tubulin
Antimitotic
Pyrimidine-benzimidazole
Cytotoxicity
Apoptosis

ABSTRACT

An approach in modern medicinal chemistry to discover novel bioactive compounds is by mimicking diverse complementary pharmacophores. In extension of this strategy, a new class of piperazine-linked cinnamide derivatives of benzimidazole-pyrimidine hybrids have been designed and synthesized. Their *in vitro* cytotoxicity profiles were explored on selected human cancer cell lines. Specifically, structural comparison of target hybrids with tubulin-DAMA-colchicine and tubulin-nocodazole complexes has exposed a deep position of benzimidazole ring into the αT5 loop. All the synthesized compounds were demonstrated modest to interesting cytotoxicity against different cancer cell lines. The utmost cytotoxicity has shown with an amine linker of benzimidazole-pyrimidine series, with specificity toward A549 (lung cancer) cell line. The most potent compound in this series was **18i**, which inhibited cancer cell growth at micromolar concentrations ranging 2.21–7.29 μM. Flow cytometry studies disclosed that **18i** inhibited the cells in G2/M phase of cell cycle. The potent antitumor activity of **18i** resulted from enhanced microtubule disruption at a similar level as nocodazole on β-tubulin antibody, explored using immunofluorescence staining. The most active compound **18i** also inhibited tubulin polymerization with an IC_{50} of 5.72 ± 0.51 μM. *In vitro* biological analysis of **18i** presented apoptosis induction on A549 cells with triggering of ROS generation and loss of mitochondrial membrane potential, resulting in DNA injury. In addition, **18i** displayed impairment in cellular migration and inhibited the colony formation. Notably, the safety profile of most potent compound **18i** was revealed by screening against normal human pulmonary epithelial cells (L132: IC_{50}: 69.25 ± 5.95 μM). The detailed binding interactions of **18i** with tubulin was investigated by employing molecular docking, superimposition and free energy analyses. Thus remarks made in this study established that pyrimidine-benzimidazole hybrids as a new class of tubulin polymerization inhibitors with significant anticancer activity.

1. Introduction

Cellular and molecular targeted cancer drug discovery can be defined by a few elementary pillars [1], one of the most imperative ones is the commencement of small-molecule inhibitors (SMIs) [2]. This advanced drug findings empowered the research to discover multiple medicinal chemistry tactics [3], wherein the design from known molecules capitalize on a lead generation campaign to identify novel hit molecules from existing structural likenesses possessing diverse chemical scaffolds in a single framework [4].

Microtubules are the enclosures of α,β-tubulin heterodimers, which are essential for the cytoskeletal assembly of normal cells as well as cancer cells with the contribution in intracellular transport, cell motility, and formation of the mitotic spindle during cell division [5]. A strong tubulin expression was regularly found in many of the tumors, such as brain tumors (85%–100%), lung cancer (35%–80%), malignant melanoma (77%), pancreatic adenocarcinoma (50%), and renal cell carcinoma (15%–80%). Therefore, timely identification of a new class of microtubule-targeting agents (MTAs) [6] is in high demand. Additionally, a noticeable number of structurally diverse natural and semi-synthetic antimitotic agents specifically paclitaxel, dolastatin 10, epothilone, colchicine (**A**, Fig. 1), combretastatin A-4 (**C**, Fig. 1), vinblastine

* Corresponding authors.
E-mail addresses: vgreddy@arizona.edu (V.G. Reddy), shankar.niperhyd@gov.in (N. Shankaraiah).

https://doi.org/10.1016/j.bioorg.2021.104765
Received 26 October 2020; Received in revised form 12 February 2021; Accepted 20 February 2021
Available online 24 February 2021

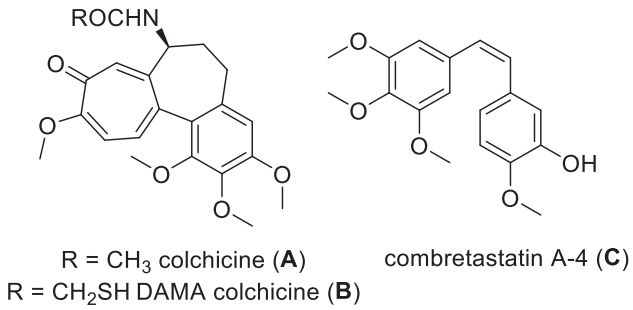

Fig. 1. Representative examples of tubulin inhibitors.

effectively targets the dynamics of tubulin depolymerization and polymerization [7,8]. However, many clinically beneficial tubulin inhibitors were constrained due to a narrow therapeutic window, complex syntheses, and purification procedures. The aforementioned compilation provokes the scientific community to explore novel antimitotic agents with the goal of answering the difficulties for gifted clinical profit in chemotherapy [9].

Small molecular entities of cancer drugs provided the courage of attaining translational outcome in the drug discovery due to the profound awareness of cellular microenvironment and multiple transduction pathways [10]. Diverse synthetic small molecules have been reported with structurally varied heteroaromatic cores, in which pyrimidine accounts for 16% of top five commonly used six-membered aromatic nitrogen-heterocycles among the U.S. FDA approved pharmaceuticals [11]. The medicinal significance of pyrimidine derivatives is promising with varied biological properties where anticancer potential can be allied with their affinity to tyrosine kinase [12], tubulin [13], phosphorylase, lysophosphatidic acid acyl transferase β(LPAAT β), histone deacetylase [14], inositol kinase, autotaxin, and heat shock protein [15] etc., Lexibulin (**D**, Fig. 2) features a pyrimidine structure, identified to target the colchicine binding site of tubulin and mode of binding was established recently by 5CA0 tubulin-lexibilun complex [16]. Similarly, aplicyanins (**E**, Fig. 2) are the first known 3-(pyrimid-4-yl)indole holding marine natural products with antimitotic properties [17]. Also, Verubulin (**F**, Fig. 2) was structurally related to fused-pyrimidine recognized through a high-throughput screening (HTS) campaign with tubulin inhibition binding at the colchicine site [18].

Moreover, conjugates derived from a combination of benzimidazole with other heterocyclic cores are considered as assisting isosters of nucleotides, illuminating the significance in chemotherapeutic applications [19]. Benzimidazole as a pharmacophore take part in numerous therapeutic areas counting HIV-RT inhibitor [20], anticancer [21], antihypertensive, antioxidant, anticoagulant [22], antihistamine, antimicrobial [23], antimalarial and antiulcer activity [24]. Denibulin derivatives (**H** and **I**, Fig. 2) are tubulin binding vascular disrupting agents with successful implication in conventional cisplatin or radiation therapy treatments [25]. Nocodazole (**J**, Fig. 2) is a natural lead product used to discover novel antimitotic agents due to its rapid interference with microtubules [26]. In addition, BAL27862 (**K**, Fig. 2) is a novel benzimidazole MTA with very potent inhibition on resistant human cancer cells [27].

Furthermore, cinnamide acts as a valuable prototype in medicinal chemistry, which is present abundantly in natural products [28] and exhibit a plethora of therapeutic applications, such as anticancer [29], antitubercular, antidiabetic, antimicrobial [30], antiviral, antiinflammatory, and antimalarial [31]. For instance, Plinabulin (**G**, Fig. 2) is a synthetic hydrophilic dicinnamide derived from a natural product, phenylahistin, which induces tubulin depolymerization by interacting at adjacent or colchicine binding site [32].

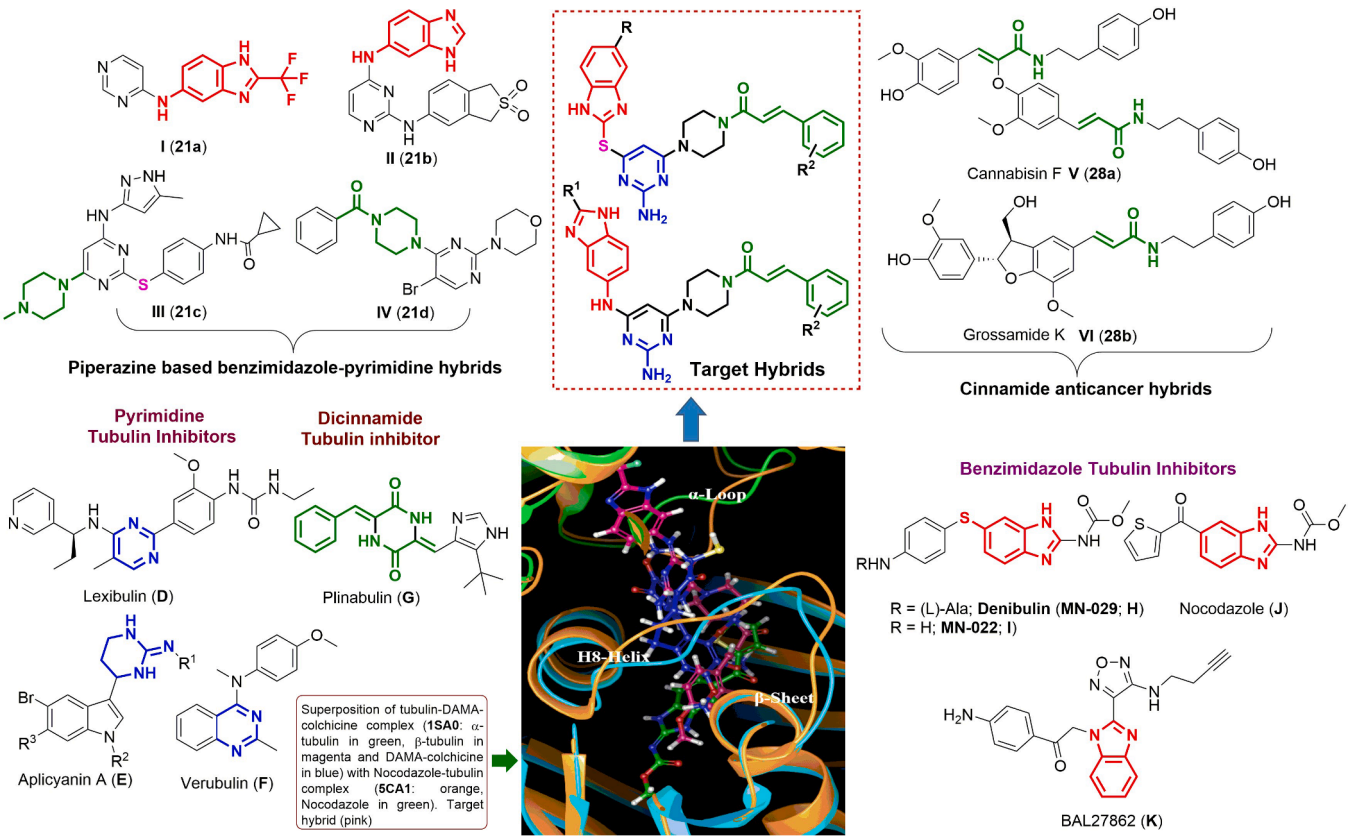

Fig. 2. Rationale and design of cinnamide derived pyrimidine-benzimidazole hybrids.

1.1. Molecular design strategy

In the vision of previous distinction, a new class of thioether and amine-bridged cinnamide derived pyrimidine-benzimidazole hybrids were designed based on the pharmacophore hybridization approach by mimicking the structural similarities of existing tubulin inhibitors. For the designed molecules, we further carried out molecular modeling studies to identify favorable binding regions and affinity by superposition of the crystal structures, tubulin-DAMA-colchicine (1SA0) and tubulin-nocodazole complexes (5CA1). When the target hybrid was superimposed onto this complex, it revealed the partial overlap of the target hybrid with a docked colchicine and nocodazole in colchicine binding domain. Peculiarly, the benzimidazole ring in the target hybrid is jagged toward α-tubulin T5 loop, acknowledged to be intricate in the gathering of tubulin $\alpha\beta$-heterodimers, signifying the incorporation of benzimidazole motif for its biological activity. The structural alteration of target hybrids comprises; (i) the modification of heteroatom attachment between pyrimidine and benzimidazole, introduced S and NH-groups; (ii) R and R^1 incorporation at the 5th and 2nd positions of benzimidazole ring presented OCH_3, $OCHF_2$, and CF_3, phenyl groups; (iii) piperazine linker attachment between pyrimidine and cinnamide rings; (iv) substitution effect of electron with-drawing/donating groups on cinnamide motif.

2. Results and discussion

2.1. Chemistry

The synthetic routes to prepare cinnamide derived thioether/amine-bridged pyrimidine-benzimidazole hybrids (**17a-u** and **18a-j**) are illustrated in Scheme 1a–c and 2. The two primary benzimidazole intermediates **3a-c** and **7a**,**b** were synthesized according to the reported procedures (Scheme 1a,b) [33]. The accomplishment of the thiol derivatives uses imidazoline cyclization between commercially available *o*-phenylene diamines and carbon disulphide to afford 1*H*-benzo[*d*] imidazole-2-thiols **3a-c**. Next, nitro substituted *o*-phenylene diamine **4** undergoes imidazoline cyclization *via* condensation reaction with substituted benzaldehydes **5a**,**b** to provide 2-substituted 5-nitro-1*H*-benzo[*d*]imidazoles **6a**,**b**. The nitro group was then reduced using mild tin chloride dihydrate to its respective amines **7a**,**b** through electron transfer reaction as shown in Scheme 1b. Furthermore, it is essential to gather an excessive amount of piperazinyl-pyrimidine intermediate **13**, in which the crucial intermediate 4,6-dichloropyrimidin-2-amine **11** (Scheme 1c) was prepared by reported procedures involving a concise two-step reaction sequence, with an overall yield of 64% [34]. Condensation reaction of diethyl malonate **8** with guanidine hydrochloride **9** utilizes sodium methoxide as a base to furnish the 2-amino-pyrimidine-4,6-diol **10** with elimination of ethanol as a byproduct. Additionally, chlorination of alcoholic groups of pyrimidine-4,6-diol was executed using $POCl_3$ as chlorine source.

Subsequently, one of the chlorine groups of 4,6-dichloropyrimidin-2-amine **11** involves nucleophilic substitution selectively with piperazine under basic reaction conditions to afford 4-chloro-6-(piperazin-1-yl)pyrimidin-2-amine **13**. Next, the 4-chloropyrimidine derivative **13** was then reacted with substituted mercaptobenzimidazoles **3a-c** as nucleophile

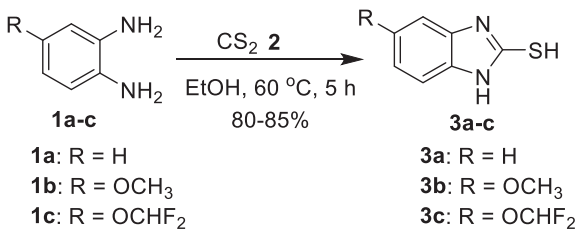

Scheme 1a. Synthesis of benzimidazole-thiol intermediates **3a-c**.

under mild acidic conditions to afford **14a-c**. Simultaneously, the monochloro derivative **13** was also reacted with 2-substituted 1*H*-benzo[*d*]imidazol-5-amines **7a**,**b** under strong acidic conditions in ethanol as a protic solvent to provide compounds **15a**,**b**. Finally, the nucleophilic nitrogen of piperazine at C6 position of benzimidazole-pyrimidines were successively coupled with substituted cinnamic acids to provide the desired hybrid molecules **17a**–**u** and **18a**–**j** (Scheme 2).

2.2. Biological evaluation

2.2.1. In vitro anticancer screening

The growth inhibitory effects of the newly synthesized hybrids **17a-u** and **18a-j** were evaluated for their *in vitro* cyctotoxicty profiles aganist four cancer cell lines using nocodazole as a reference standard (Table 1). Those were A549 (human lung cancer), PC-3 (human prostate cancer), HeLa (human cervical cancer), and MDA-MB-231 (human breast cancer) in which, the cell viability (IC_{50}) was determined using 3-(4,5-dimethylthiazol-2-yl)-2,5-diphenyltetrazolium bromide (MTT) protocol [35]. The preliminary results of the study revealed that all the titled compounds exhibited significant tumor cell growth inhibition against lung cancer cell line (A549), 14 compounds namely **17b**, **17d**, **17f**, **17l**, **17m**, **17o**, **17r**, **17u**, **18d-f**, **18h-j** have displayed promising cytotoxicity with IC_{50} values 2.21 ± 0.12 μM to 9.18 ± 1.18 μM. The rest of the compounds have showed modest antiproliferative activity with IC_{50} values ranging from 10.40 ± 0.74 μM to 22.41 ± 3.84 μM. The hybrids featuring amine linker provides better antiproliferative activity in all the selected cell lines. Remarkably, one of the verified compounds, **18i**, bearing a more sterically hindered trifluoromethyl group at *C*2 position of benzimidazole ring unveiled superior *in vitro* cytotoxic potential against lung cancer cell line (A549) with IC_{50} value 2.21 ± 0.12 μM. It is also evident that compound **18i** was revealed to be active with the corresponding IC_{50} values 3.15 ± 0.41 μM, 7.29 ± 0.67 μM and 5.71 ± 1.14 μM against prostate (PC-3), breast (MDA-MB-231), and cervical (HeLa), respectively. It could be pragmatic from the IC_{50} values that the compound **18j** holding fluorine substituent on cinnamide functionality was found to bring growth inhibition of lung (A549), prostate (PC-3), breast (MDA-MB-231), and cervical (HeLa) cancer cells with 50% inhibition at 5.18 ± 0.72 μM, 8.37 ± 0.65 μM, 11.43 ± 0.83 μM and 6.12 ± 0.46 μM, respectively. Moreover, most of the synthesized compounds demonstrated good to moderate antitumor activity on lung (A549), prostate (PC-3), breast (MDA-MB-231), cervical (HeLa) with IC_{50} values 2.21–21.8 μM and overhead.

As shown in Table 1, the new hybrids featuring thioether linker displayed the substantial cancer cell growth inhibition, slightly being less active than the amine linker hybrids. In exact, amid 20 molecules, 5 compounds namely **17b**, **17h**, **17m**, **17t**, and **17u** revealed effective *in vitro* cytotoxicity owning less than 10 μM IC_{50} (i.e., 6.21–8.78 μM) against HeLa cervical cancer cells. Moreover, compounds **17e**, **17h**, **17m**, **17r**, **17t**, and **17u** presented a noteworthy *in vitro* antiproliferative activity against MDA-MB-231 triple-negative breast cancer (TNBC) cell line with IC_{50} values 6.94 to 9.34 μM. Compounds **17m** (IC_{50} 6.53–10.41 μM) and **17r** (IC_{50} 6.94–10.42 μM) were found to exhibit superior cytotoxic effects against all the tested cell lines with IC_{50} value around 10 μM. Likewise, thorough inquiry of the IC_{50} values specified that antitumor ability of 9 compounds **17b**, **17d**, **17f**, **17l**, **17m**, **17o**, **17r**, and **17u** lean toward lung cancer cell lines with IC_{50} values 5.17–10.41 μM. Moreover, the most potent compound **18i** revealed 69.25 ± 5.95 μM IC_{50} against normal human pulmonary epithelial cells (L132) with maximum safety profile. It could be perceived from the *in vitro* antiproliferative activity that both compound series were evinced to be contribute in advancing new anti-cancer agents against lung cancer. Depending on the key results realized, the most bioactive compound **18i** was voted for further mechanistic investigations to comprehend the hidden antitumor mechanisms.

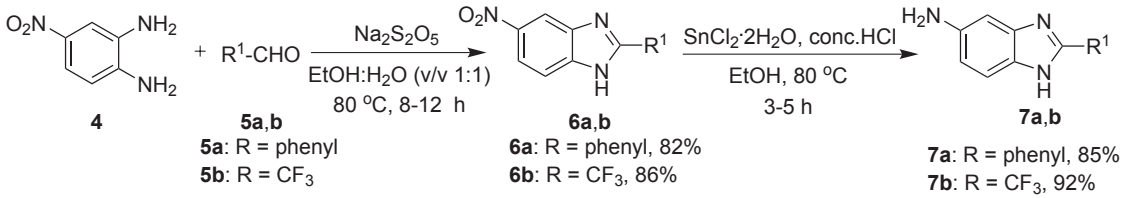

Scheme 1b. Synthesis of benzimidazole-amine intermediates **7a,b**.

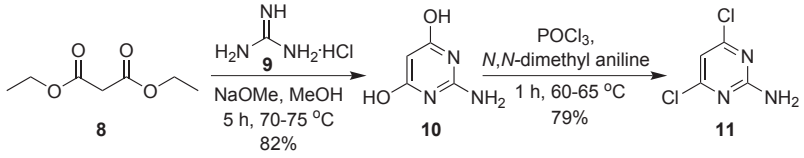

Scheme 1c. Synthesis of dichloro derivative of pyrimidine intermediate **11**.

2.2.2. Structure activity relationship (SAR)

Structure activity relationship (SAR) is composed from the results attained in relation to the heteroatom nature of benzimidazole attachment to the pyrimidine motif, and the position and electronic nature on phenyl ring of cinnamide group. It can be observed by relating the respective data for **17a-u** and **18a-j** molecular series, the hetero atom nature of benzimidazole to the pyrimidine ring influenced the activity of the pertinent compounds, those belonging to the amine (**18a-j**) series were more active on A549 cancer cell line than the corresponding thioether (**17a-u**) hybrids (e.g., compare IC_{50} (**18i**) = 2.21 μM and IC_{50} (**17t**) = 22.41, Table 1). In view of A549 cell line as concept validation with respect to the amine linker derivatives, the presence of dual electronic nature i.e., electron with-drawing (CF_3; **18f**, **18h-j**; IC_{50}: 2.21 – 9.18 μM) and electron donating (phenyl; **18a**, **18c-f**; IC_{50}: 5.61–16.33 μM) at C2-positon of benzimidazole were found to be tolerable, in which the later were less active to some extent. Also, for thioether compound series (**17a-u**), the existence of the neutral (H; **17a-g**), electron donating (OCH_3; **17h-n**) or electron with-drawing ($OCHF_2$; **17o-u**) equally influenced the antiproliferative activity with moderate inhibition.

On the other hand, with regard to cinnamide motif, substitution featuring bulkier group such as 2-bromo-4,6-dimethoxy and 2-bromo-4-methoxy were proved to be endurable in both the molecular series (**17f**, **17l**, **17t**, **18c**, and **18i**), of which **18i** was ascertained to be the most significant one. The well-known 3,4,5-trimethoxy structural setting on the cinnamide skeleton exhibited moderate activity of subsequent compounds **17c**, **17r**, and **18h** particularly to A549 cell line, HeLa and MDA-MB-231. Although, compound **18b** seemed to be an exception, holding the activity towards PC-3 cell line. However, compound **17s** with substitution of biphenyl as larger steric group displayed a diminished bioactivity toward all the cell lines. Attachment of caffeic acid ring on piperazine (**17d**) shifted the activity to A549 cell line and a non-significant activity was spotted on rest of the cell lines. Similarly, incorporation of strong electron with-drawing 4-nitro group (**17g**, **17n**) led to a diminution in the antiproliferative activity of all the tested cancer cell lines (Fig. 3).

*2.3. Effect of **18i** on tubulin polymerization inhibition*

To inspect the effect of **18i** on microtubules [7d], the tubulin polymerization inhibitory potential was assessed at diverse concentrations (8, 4, 2, 1, 0.5 μM) with combretastatin 3 μM and paclitaxel 3 μM) aiding as positive controls. The G2/M phase cell cycle arrest in cancer cells is often accompanied with the tubulin polymerization inhibition. Hence, to understand the obscured mechanism of the potent compound **18i**, we performed cell-free *in vitro* tubulin polymerization assay by observing the rate of fluorescence emission at 440 nm (excitation wavelength is 360 nm) for 1 h at 37 °C (Fig. 4**a**). The experiment was executed in duplicates and from the Fig. 4**b**, it was inferred that 28.4%, 33.5%, 78.2% of tubulin polymerization were observed in the treatment group of **18i** at the concentrations of 2, 4.0, and 8.0 μM, respectively, compared to the vehicle group (DMSO). Fortunately, the compound **18i** exhibited significant tubulin polymerization inhibition with an IC_{50} value of 5.72 ± 0.51 μM and interrelated well with the anti-tumor potency, supporting that the tubulin polymerization inhibition by **18i** is in a dose-dependent manner.

2.4. Anti-microtubulin effects by immunofluorescence staining

To gain the insights of microtubulin disrupting effects, a cell-based phenotypic assay was performed on compound **18i** aganist A549 lung cancer cell line. The architect features of the microtubule were scrutinized using an anti-*β*-tubulin antibody by immunofluorescence staining [36]. To recognize the basic mechanism of **18i** interaction with tubulin, the A549 cells were treated with compound **18i** and nocodazole as a positive control and stained for DNA (blue) and *β*-tubulin (green). The microtubule grid unveiled standard frame-up and assembly in A549 cells in DMSO-treated control cells. However, exposure with compound **18i** at 2 and 4 μM doses directed to dramatic destruction of microtubule network in A549 cells. The microtubule configuration turned out to be progressively chaotic, exhibiting clear signs of apoptosis with increased concentartion in the **18i** treatment group. Parallel results also detected when the cells were treated with nocodazole at 2 and 4 μM. These fallouts suggested that compound **18i** inhibited microtubule formations in a concentration dependent mode through direct binding with tubulin component as shown in Fig. 5.

3. Computational studies

3.1. Molecular docking

Using the crystalline intricate of DAMA colchicine binding tubulin (PDB ID: 1SA0) [37], the possible binding mode of the most potent cytotoxic compound, **18i,** was investigated by a series of molecular modelling studies in the colchicine binding domain. The projected binding mode of **18i** virtually macthes the DAMA colchicine as presented in Fig. 6**a**. Three well distinct regions enfold compound **18i** as exposed in Fig. 6**b**: region 1, cinnamide ring: positioned deep in the hydrophobic pocket of *β*-subunit; region 2, pyrimidine-piperazine: bridge between *α*–and *β*–subunits; region 3, where the benzimidazole ring placed inside the *α*-subunit. The free amino bridge between

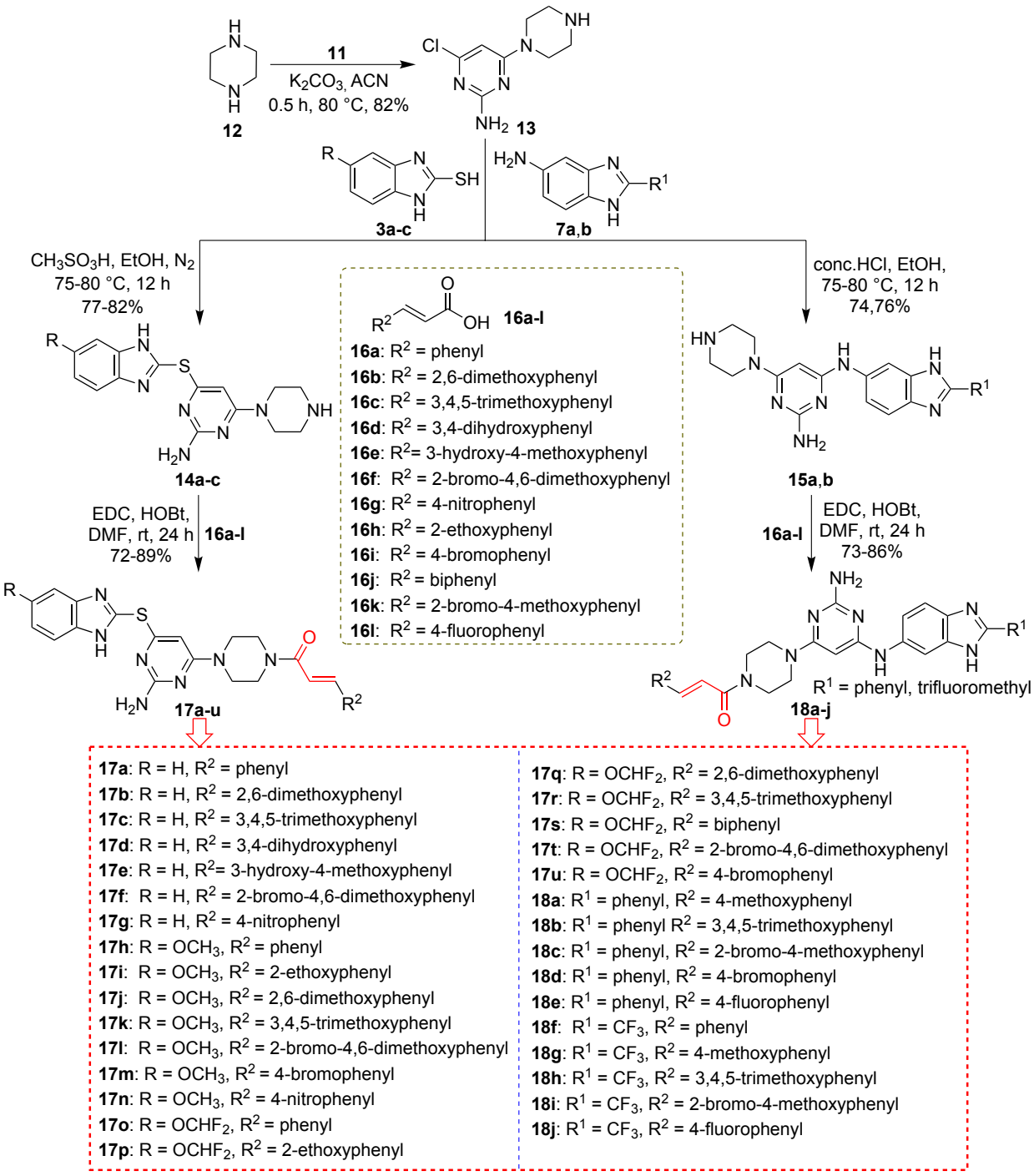

Scheme 2. Design and synthesis of cinnamide derived thioether/amine-bridged pyrimidine-benzimidazole hybrids **17a-u** and **18a-j**.

benzimidazole and pyrimidine motifs interact with αThr-179, possibly locking the compound in this favorable binding configuration. A trigonal shape aromatic hydrogen bond was identified between hydrogens of benzimidazole phenyl ring and carbonyl group of αAsn101. Interestingly, the benzimidazole ring was deeply penetrated into the α-tubulin T5-loop, highlighting the incorporation for biological significance. The cinnamide ring of compound **18i** was intensely hidden in to the hydrophobic pocket molded by residues βTyr202, βVal238, βCys241, βLeu242, βLeu255, βAla316, βAla317, βVal318, βAla354, and βIle378.

To expand our results, we tried the superimposition of potential ligand **18i** with DAMA colchicine and nocodazole as represented in Fig. 7**a & b**. The ensuing superimposition posture of DAMA colchicine revealed the partial overlap of pyrimidine-piperazine motif with ring B, whereas the cinnamide functionality covered the lower portion of the trimethoxy phenyl ring. On the other hand, nocodazole being a small molecule showed less overlapping with ligand **18i**, but occupied a similar binding site. Finally, the superimposition of all the three ligands exhibited similar binding pose at colchicine binding site of α/β-tubulin protein as perceived in Fig. 7**c**.

3.2. *In silico ADME/T and prime MM/GBSA binding energy studies*

QikProp program of Schrödinger software was used to study drug-

Table 1
In vitro cytotoxicity (IC_{50})[a] of carbamide derivatives **17a-u** and **18a-j** against diffrent human cancer cell lines by MTT assay.

Entry	A549[b]	PC-3[c]	HeLa[d]	MDA-MB-231[e]	L132[f]
17a	11.1 ± 0.61	20.21 ± 3.53	>25	11.45 ± 2.11	ND
17b	**5.2 ± 0.41**	12.52 ± 1.65	**8.78 ± 1.12**	17.68 ± 1.42	ND
17c	10.41 ± 0.74	16.21 ± 0.74	>25	>25	ND
17d	**6.12 ± 0.93**	>25	14.18 ± 1.71	>25	ND
17e	>25	14.18 ± 3.12	12.92 ± 2.36	**8.25 ± 1.91**	ND
17f	**5.42 ± 0.21**	**9.49 ± 1.21**	10.14 ± 0.91	>25	ND
17g	18.62 ± 0.48	>25	>25	13.27 ± 2.16	ND
17h	13.18 ± 0.77	18.19 ± 2.15	**7.39 ± 1.29**	**9.34 ± 0.75**	ND
17i	16.14 ± 1.84	11.13 ± 0.98	>25	21.21 ± 3.51	ND
17j	>25	>25	22.74 ± 3.24	>25	ND
17k	>25	>25	19.45 ± 2.38	11.71 ± 1.31	ND
17l	**6.11 ± 2.18**	**8.13 ± 2.71**	>25	13.53 ± 2.72	ND
17m	**8.35 ± 0.41**	10.41 ± 1.77	**6.53 ± 1.21**	**7.31 ± 1.27**	ND
17n	12.45 ± 1.16	>25	18.21 ± 2.14	>25	ND
17o	**5.17 ± 0.83**	15.31 ± 2.21	12.14 ± 2.16	22.94 ± 2.31	ND
17p	>25	>25	22.73 ± 3.48	>25	ND
17q	15.41 ± 2.23	**6.32 ± 0.78**	>25	**9.12 ± 1.82**	ND
17r	**7.11 ± 0.44**	>25	10.42 ± 1.46	**6.94 ± 1.16**	ND
17s	>25	>25	19.78 ± 3.12	18.11 ± 1.58	ND
17t	22.41 ± 3.84	11.46 ± 1.89	**8.57 ± 1.54**	>25	ND
17u	**8.14 ± 0.51**	14.21 ± 2.91	**6.21 ± 0.87**	**8.32 ± 1.51**	ND
18a	16.33 ± 2.15	**7.94 ± 1.69**	**9.43 ± 1.17**	>25	ND
18b	>25	**5.81 ± 0.97**	13.1 ± 1.52	15.14 ± 2.14	ND
18c	12.44 ± 1.56	11.19 ± 0.67	21.34 ± 1.57	>25	ND
18d	**8.93 ± 1.56**	>25	15.49 ± 2.15	12.18 ± 1.47	ND
18e	**5.61 ± 1.88**	**4.82 ± 0.71**	>25	**7.42 ± 1.15**	ND
18f	**7.28 ± 1.94**	21.8 ± 3.13	>25	11.54 ± 2.11	ND
18g	>25	13.52 ± 2.17	11.67 ± 1.98	>25	ND
18h	**9.18 ± 1.18**	>25	**8.23 ± 1.27**	15.34 ± 1.18	ND
18i	**2.21 ± 0.12**	**3.15 ± 0.41**	**7.29 ± 0.67**	**5.71 ± 1.14**	69.25 ± 5.95
18j	**5.18 ± 0.72**	**8.37 ± 0.65**	11.43 ± 0.83	**6.12 ± 0.46**	ND
Nocodazole[g]	2.39 ± 0.14	1.96 ± 0.24	3.48 ± 0.52	2.13 ± 0.25	ND

Data represent the average of three independent experiments performed in quadruplet.
ND- Not determined.
[a] IC_{50} values are the concentrations (μM) that cause 50% inhibition of cancer cell growth.
[b] Human lung cancer cell line.
[c] Human prostate cancer cell line.
[d] Human cervical cancer cell line.
[e] Human breast cancer cell line
[f] Human pulmonary epithelial cells.
[g] Reference compound.

likeliness, physicochemical and pharmacokinetic crucial properties [38] of potent compound **18i** and known tubulin inhibitors colchicine and nocodazole as outlined in Table 2. This *in silico* study describes that the synthesized hybrid **18i** has suitable logP values with no violation in the permitted ranges of physico-chemical descriptors. The purpose of MM-GBSA docking analysis in the current effort is to observe the ligand-protein affinity and complexation energy to α/β-tubulin [39], thus giving more insights regarding the pose and pattern of interactions. The most active ligand **18i** confirmed greater binding energy than colchicine and nocodazole, suggesting stronger binding for steady ligand-protein complex establishment.

4. Analysis of cell cycle effect

Quantification of cellular DNA content by flow cytometry was one of the initial applications to detect the growth inhibitory potential of antitumor agents on specific cell cycle check-points [40]. The dose-response effects of the most active compound **18i** on cell cycle progression was measured on A549 cells after incubation with compound **18i** (1, 2 and 4 μM) for 48 h. The flow cytometry outcome of PI-stained cultures demonstrated the induction of noteworthy upsurge in G2 phase cell population. As signified in Fig. 8, blockade of cell cycle arrest in G2 phase was accompanied in a dose dependent manner with comparable reduction in G1 and S phases. The cell population in G2/M phase was enhanced by 15–35%, specifying the ability of the compound infusion of incubated cells through G2/M phase. Finally, the results established the capability of compound **18i** as antimitotic agent.

4.1. Wound healing assay (migration assay)

Pathological conditions such as cancer and inflammation cause dysregulation of cell migration, a vital process for embryonic development, tissue injury, and wound healing. Wound healing assay is a 2D cell migration approach, used for measuring rate of gap closure i.e., the rapidity of communal motion of the cells [41]. The migration ability of compound **18i** was examined by the execution of wound healing assay on human umblical vein endothelial cells (HUVECs). In this procedure, a "wound gap" was created by scraping with a sterile pipette tip on extremely metastases coalescent cell monolayers of HUVECs and the closure of the wound was monitored using phase contrast microscopy. As revealed in Fig. 9, the 30 h treatment of compound **18i** at increased concentrations of 1, 2 and 3 μM, exhibited extensive inhibition of cell migration in a dose dependent manner compared to the control cells. Also, quantification of the healed area with cells were analyzed by the Wimasis WimScratch software which has shown the significant decrease from 97.9 to 87.8% of cell-covered area with treated concentrations of compound **18i** (**Fig. S1 and S2**).

4.2. Colony forming assay

Adhesion-independent progression is the ability of a solo adherent cell to form a multiple of colonies, and is a hallmark of carcinogenesis. Colony formation assay is a well-established method for illustrating this capability *in vitro* and is reflected to be one of the most stringent tests for cancerous alteration in cells [42]. In this protocol, the cell evolution of A549 subpopulations in the adhesion-independent condition was measured at increased doses (1, 2 and 4 μM) of compound **18i**. The proliferative capacity of the treated cells can be visualized by staining with crystal violet. From Fig. 10, it certainly guides the inhibitory potential of **18i** on colony forming ability of A549 cells in a dose dependent manner as compared to the control. The established outcome could be one of the mechanisms reflected in provoking cytotoxic activity in A549

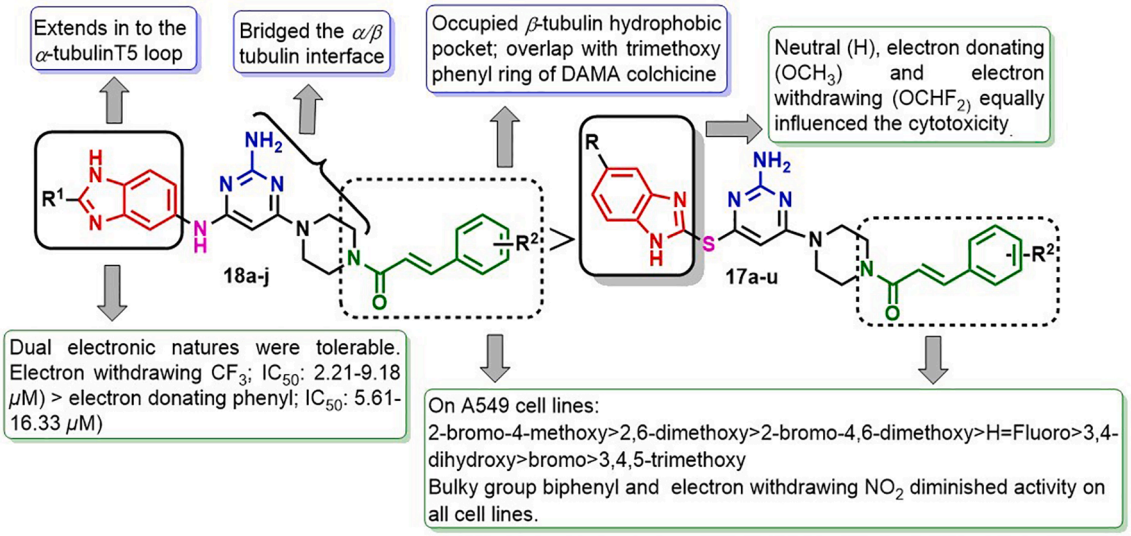

Fig. 3. SAR studies and binding mode insights of new hybrids **17a-u** and **18a-j**.

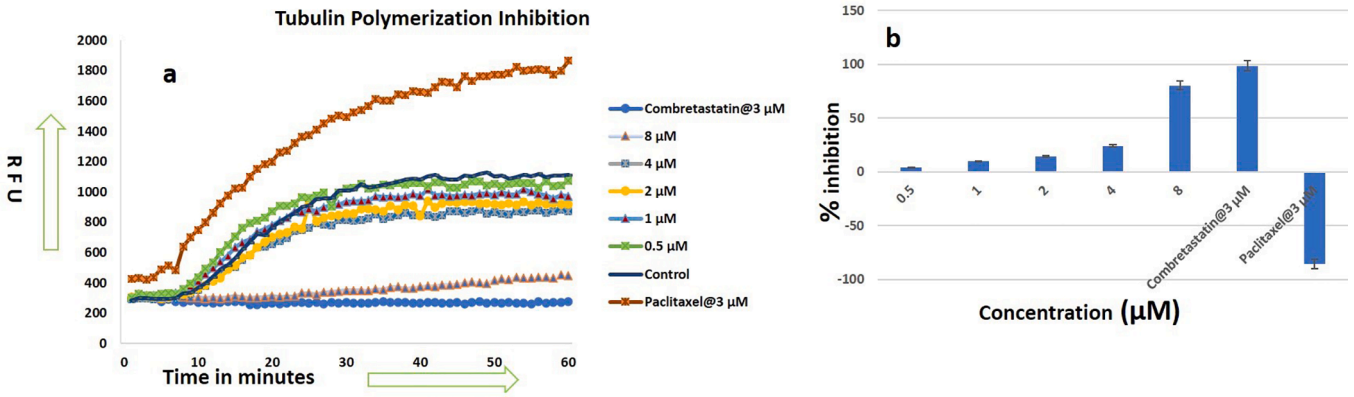

Fig. 4. a) Effect of compound **18i** on the tubulin polymerization: tubulin polymerization was monitored by the increase in fluorescence at 360 nm (excitation) and 440 nm (emission) for 1 h at 37 °C. **b**) % Dose-response inhibition of tubulin polymerization by compound **18i** at final concentrations of 8, 4, 2, 1, 0.5 μM. Combretastatin and paclitaxel, were used as reference standards. Data expressed as mean ± SEM (n = 3).

lung cancer cells.

5. Apoptosis detection studies

5.1. Nuclear morphological analysis

Cellular suicide or apoptosis with inappropriateness is considered as a vital factor in human conditions such as cancer, autoimmune disorders, neurodegenerative diseases, and ischemic damage. The progression of programmed cell death is generally characterizd by distinct morphological hallmarks including chromatin condensation, nuclear fragmentation and pyknosis. Hoeschst is a part of blue fluorescent bis benzimide dye, specific for DNA with the ability of distinguishing the nuclei of living or fixed cells and tissues. The dye binds to the minor grove of DNA with fondness towards adenine-thymine (A-T) regions. This binding enables the identification of disparity among compact chromatin of apoptotic nuclei and sort out the cells based on their DNA content [43]. In this regard, A549 cells were exposed to 1, 2 and 4 μM concentrations of compound **18i** and stained with Hoechst 33,242 to study the usual apopptotic features. As evident in Fig. 11, the 1 and 2 μM treated A549 cells resulted in condensation of the nuclei and seemed brightly than the control cells. The 4 μM treated cells caused both condensation and fragmentation of the nuclei supporting the concentration dependency in apoptosis induction of compound **18i**, where the apoptotic cells arise out as brighter than the intact control cells showing normal morphology.

5.2. Effect on mitochondrial membrane potential (DΨm)

The stability of mitochondrial membrane potential (DΨm), spawned during oxidative phosphorylation is supposed to be a requisite for healthy cell functioning. DΨm is a driving force for the synthesis of ATP and also for transport of redox compounds and proteins which are a prerequisite for cell viability [46]. Thus, it is the purpose of section for determining the sustainability of mitochondria participating in a method of dismissal of deactivated mitochondria. The changes in DΨm was monitored by fluorescence microscopy using the mitochondrial specific dye- rhodamine 123. A549 cells were exposed to proportional concentrations 1, 2 and 4 μM of compound **18i**. The disruption of DΨm is observed in association with a marked shift in fluorescence in a dose-dependent manner in correlation with control cells. Finally, from the Fig. 12, it is established that compound **18i** instigated a concentration-dependent dissipation of DΨm.

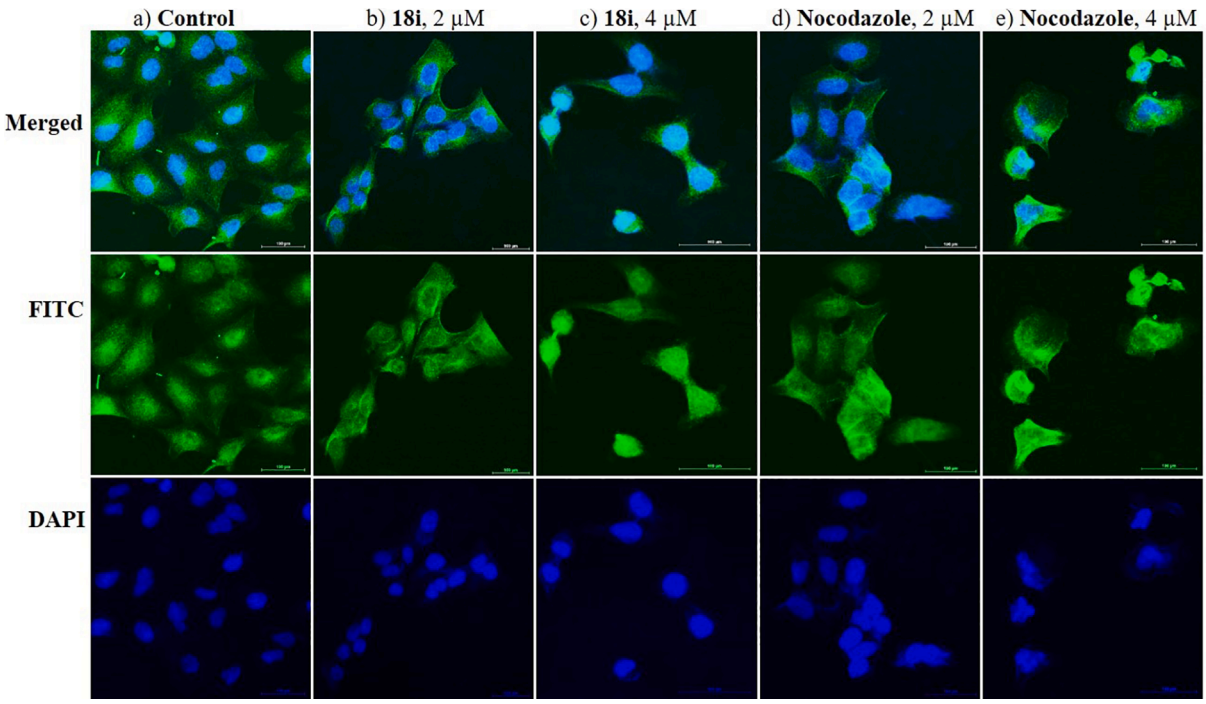

Fig. 5. Immunohistochemistry analysis of compounds on microtubule networks. A549 cells were independently treated with **18i** and nocodazole at 2 and 4 μM, respectively for 48 h. The images were captured with confocal microscope. Scale bar represents 100 μm.

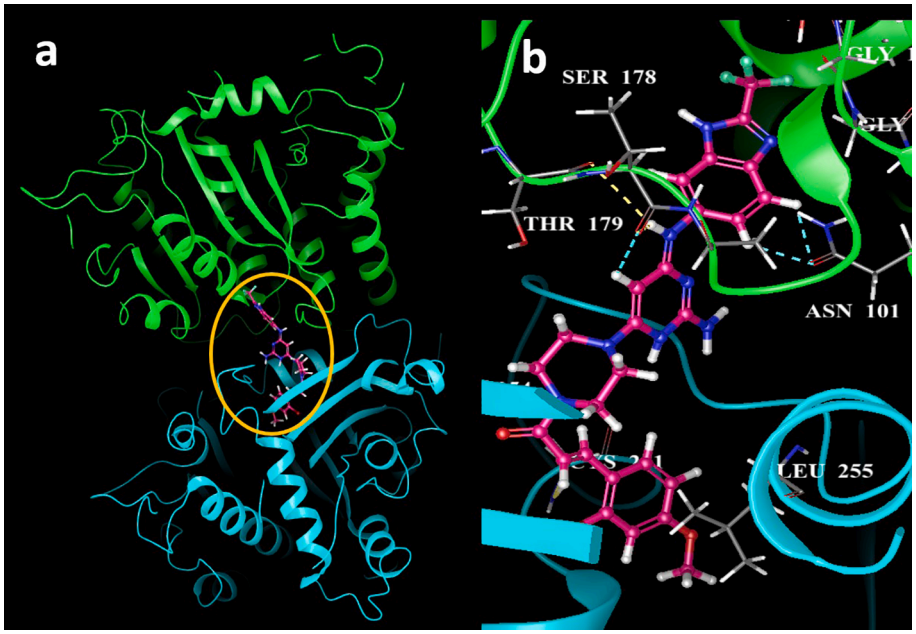

Fig. 6. a) Docking model of most potent compound **18i** and b) its ligand interactions in the colchicine binding site of α/β-tubulin (PDB ID: 1SA0). The yellow and cyan dashed lines represent hydrogen bond and aromatic hydrogen-bonding respectively: The potential ligands were shown as ball and stick model, while the interacting aminoacids were denoted as thin tubes and compound **18i** was shown as green ball and stick model in the black background. (For interpretation of the references to colour in this figure legend, the reader is referred to the web version of this article.)

5.3. *Effect on intracellular ROS generation*

Disorder of cellular redox equilibrium is a menace for the progression of several pathologies. Cancer cells express disproportional increase in reactive oxygen species (ROS) due to oncogenic alteration counting variation in metabolic, genetic, and tumor microenvironment. Perpetual boosted ROS levels have cytotoxic effects, bringing the stimulation of apoptotic pathways or obstructing resistance to chemotherapy [47]. Hence, targeting redox mechanisms tangled in cancer advancement is a potential tactic to avoid cancer. Thus, induction of ROS generation driven by the compound **18i** at varied doses 1, 2 and 4 μM in A549 cells were scrutinized using the cell permeant fluorogenic 2′,7′-dichlorodihydrofluorescein diacetate (carboxy H2DCFDA) dye. The green fluorescence produced is directly proportionate to the quantity of oxidized DCFDA to DCF revealing the cleavage of the acetate groups by intracellular oxidation and esterases. A concentration dependent ROS induction was realized by compound **18i** as pictured in Fig. 13, and therefore it could be the indicator for provocation of apoptosis of A549 lung cancer cells.

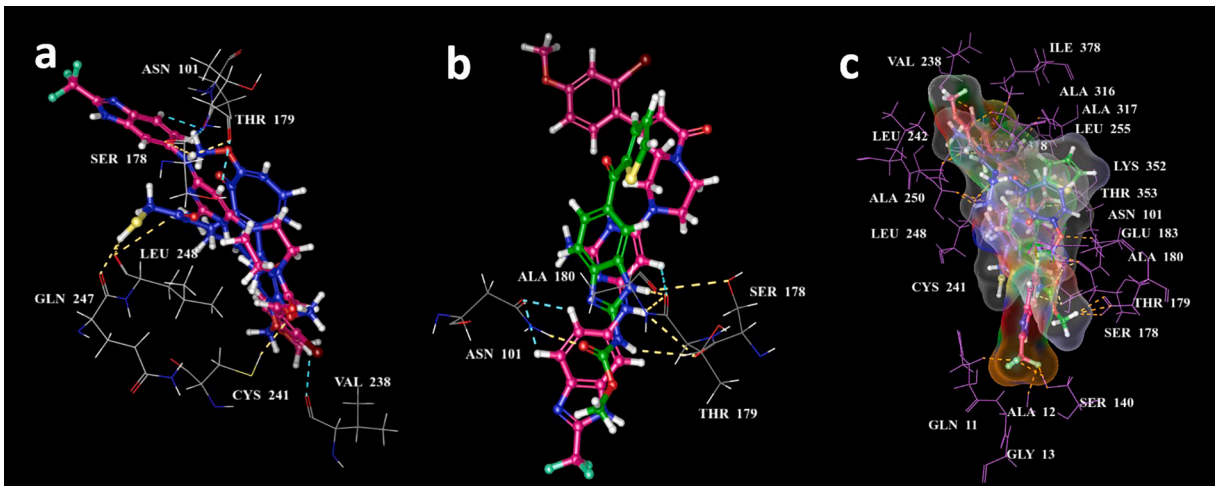

Fig. 7. a) Poses represent the superimposition of potential ligand **18i** (pink) and DAMA Colchicine (blue); b) Poses represent the superimposition of potential ligand **18i** and nocodazole (green); c) Surface representation of **18i** with DAMA and nocodazole with possible interactions in the colchicine binding site of α/β-tubulin: The potential ligands were shown as ball and stick model, while the interacting amino acids were denoted as thin tubes. (For interpretation of the references to colour in this figure legend, the reader is referred to the web version of this article.)

Table 2
ADME/T profile and binding energy of compound **18i** and tubulin inhibitors.

Entry	Descriptors	Recommended values	Ligand ID		
			18i	Nocodazole	DAMA Colchicine
1	Molecular weight	130.0–725.0	617.427	301.319	431.503
2	Dipole moment	1.0–12.5	7.996	4.922	3.776
3	Total SASA	300–1000	913.999	557.885	662.011
4	No. of rotatable bonds	0–15	7	4	7
5	Donor HB	0.0–6.0	4.000	1.000	0.800
6	Acceptor HB	2.0–20.0	8.750	5.000	7.000
7	QP Polarizability	13.0–70.0	57.203	31.126	39.448
8	QP logP o/w	2.0–6.5	4.999	3.117	3.498
9	QP log BB	−3.0 and 1.2	−1.172	−1.280	−1.792
10	Human Oral Absorption	1–3	1	3	3
11	Percent Human Oral Absorption	> 80% is high	82.027	81.551	100
12	Rule of Five violations	>25% is low	1	0	0
13	**Binding Energy (-kcal/mol)**		−51.020	−33.846	−41.818

5.4. Quantification of apoptosis induction

Annexin V-FITC/Propidium iodide assay is a biparametric cyto-fluorimetric analysis which can provide the divergence between live cells (Q4-LL; AV-/PI−), early apoptotic cells (Q3-LR; AV+/PI-), late apoptotic cells (Q2- UR; AV+/PI+), and necrotic cells (Q1-UL; AV−/PI+) [44]. In this assay, the term "biparametric" denotes the staining of DNA and phosphatidylserine (PS) residues by propidium iodide (PI) and annexin-V-FITC respectively, which exemplifies the means of cell death induced [45]. The concentration-dependent treatment of A549 lung cancer cells with compound **18i** displayed the build-up of annexin-V positive cells in a dose-dependent manner, suggesting the existence of apoptosis. As depicted in Fig. 14, the total number of late and early apoptotic cells extensively heightened to 23.5% and 34.1% in contrast to the untreated control cell population 2.55 and 5.45 respectively. These findings deep-rooted the ability of **18i** to induce cell death on A549 lung cancer cells.

6. Conclusion

In conclusion, this work demonstrates a new series of 31 piperazine-linked cinnamide derived benzimidazole-pyrimidine hybrids were designed and synthesized based on the structural platform of known tubulin inhibitors. The superposition of target hybrids with DAMA colchicine-tubulin and nocodazole-tubulin complexes revealed a deep interring of benzimidazole ring in to the α-tubulin with a conformational change in αT5 loop. SARs perceived for members of this series exposed that the existence of a NH group, positioned between benzimidazole and pyrimidine backbone, is vital for antiproliferative activity. From the primary screening, it was revealed that compound **18i** holding 2-bromo-4-methoxy substitution, displayed potent antitumor activity, with IC_{50} values ranging from 2.21 to 7.29 μM in a varied set of human cancer cell lines from different organs. Furthermore, compound **18i** inhibited tubulin polymerization by 50% at a concentration of 5.72 ± 0.51 μM in an *in vitro* assay with antimitotic properties. The cytotoxic effects of **18i** in A549 cells were correlated with induction of apoptosis mediated by dissipation of mitochondrial membrane potential, amplified ROS production with consequent DNA damage. Additionally, clonogenic and wound healing assays specified the impairment of colony formation and cell migration by **18i** in a concentration-dependent manner. Immunofluorescence study of compound **18i** revealed enhanced disruption of microtubule assembly and therefore halted the cells at G2/M phases of the cell cycle. Finally, *in silico* studies of active compound revealed the occupancy of cinnamide in to the β-hydrophobic pocket with similar binding pattern as colchicine in the α/β-tubulin protein. Thus, the synthesized new class of pyrimidine-benzimidazole hybrids pave a direction for the exploartion of new binding regions in the colchicine binding domain and with further apt structural alterations will advance new

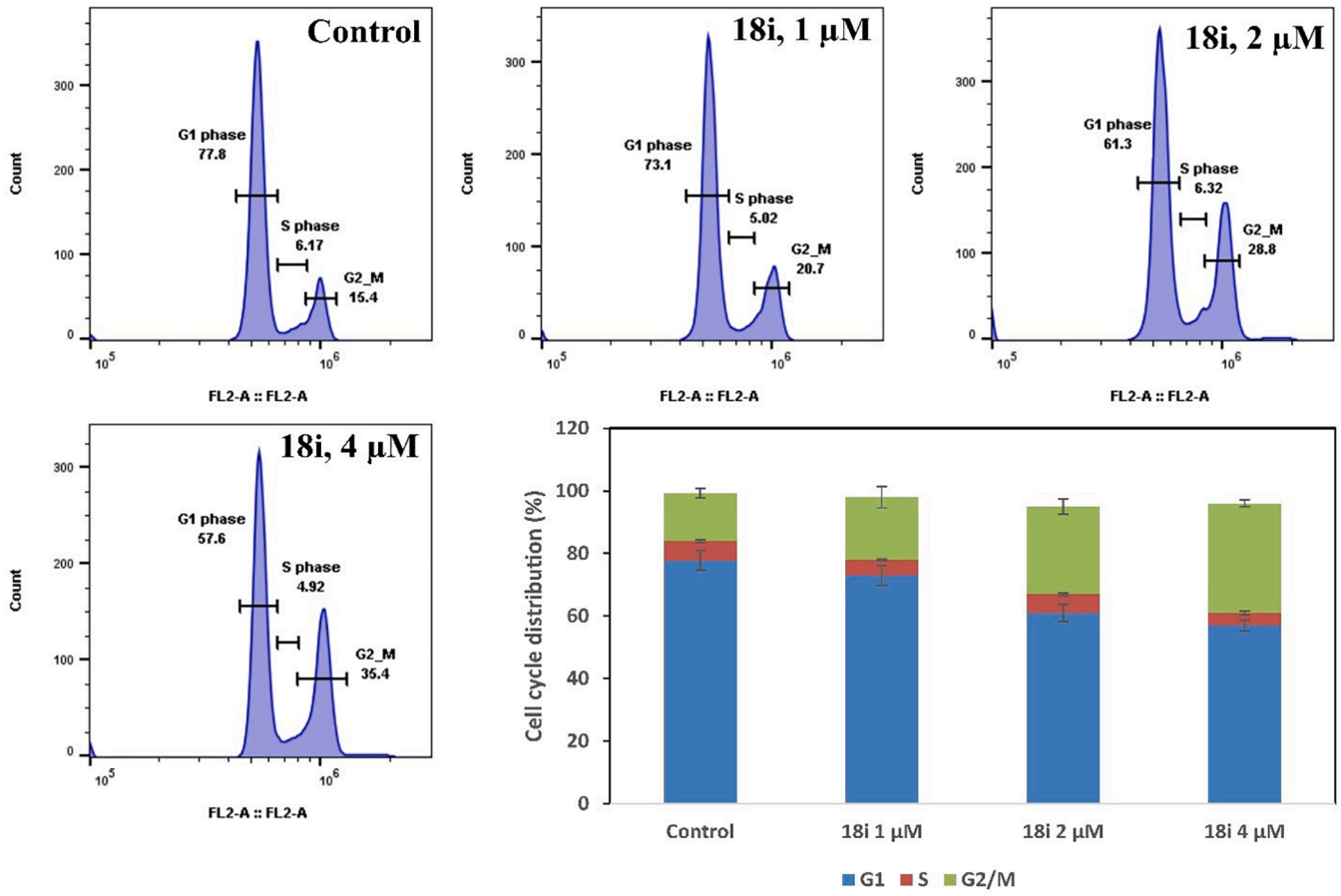

Fig. 8. Cell cycle distribution of A549 cells after treatment with compound **18i** for 48 h. The cell cycle assay was performed by propidium iodide (PI) staining method and analysed the flow cytometry data by FlowJo software.

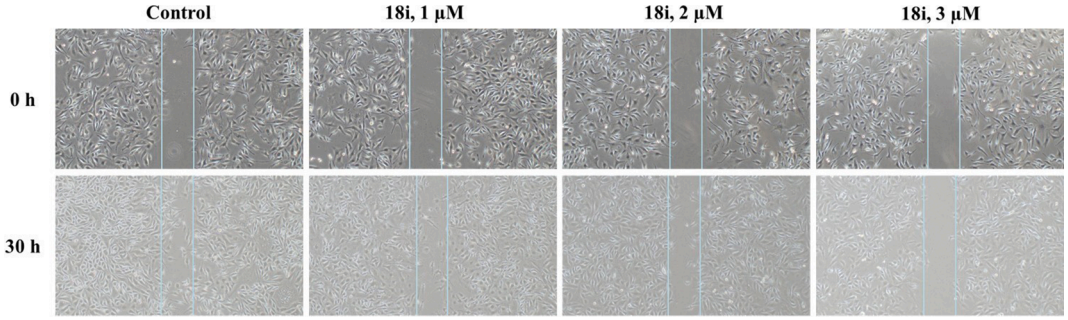

Fig. 9. Effect of compound **18i** on HUVEC cell migration. The cells were cultured in the absence and presence of compound **18i**. The wounds were created in a confluent monolayer of HUVEC with sterile micro pipette tip. The images were captured by using phase contrast microscopy at 0 h and 30 h.

generation of tubulin inhibitors in chemotherapy.

7. Experimental section

7.1. Chemistry

General methods. All the reagents and solvents were obtained from commercial suppliers and were used without further purification. Analytical thin layer chromatography (TLC) was performed on MERCK pre-coated silica gel 60-F254 (0.5 mm) aluminum plates. Visualization of the spots on TLC plates was achieved by UV light. ^{1}H and ^{13}C NMR spectra were recorded on Bruker 500 MHz by making a solution of samples in the DMSO-d_6 as solvent using tetramethylsilane (TMS) as the internal standard. Chemical shifts for ^{1}H and ^{13}C are reported in parts per million (ppm) downfield from tetramethylsilane. Spin multiplicities are described as s (singlet), brs (broad singlet), d (doublet), t (triplet), q (quartet), and m (multiplet). Coupling constant (*J*) values are reported in *hertz* (Hz). HRMS were determined with Agilent QTOF mass spectrometer 6540 series instrument. Wherever required, column chromatography was performed using silica gel (60–120; 100–200). The reactions were conducted under anhydrous conditions and when required are carried under nitrogen positive pressure using freshly distilled solvents. All evaporation of solvents was carried out under reduced pressure using a rotary evaporator below 45 °C. Melting points were determined with an electro thermal digital melting point apparatus IA9100 and are uncorrected. The names of all the compounds given in the experimental section were taken from ChemBioDraw Ultra, Version 12.0.

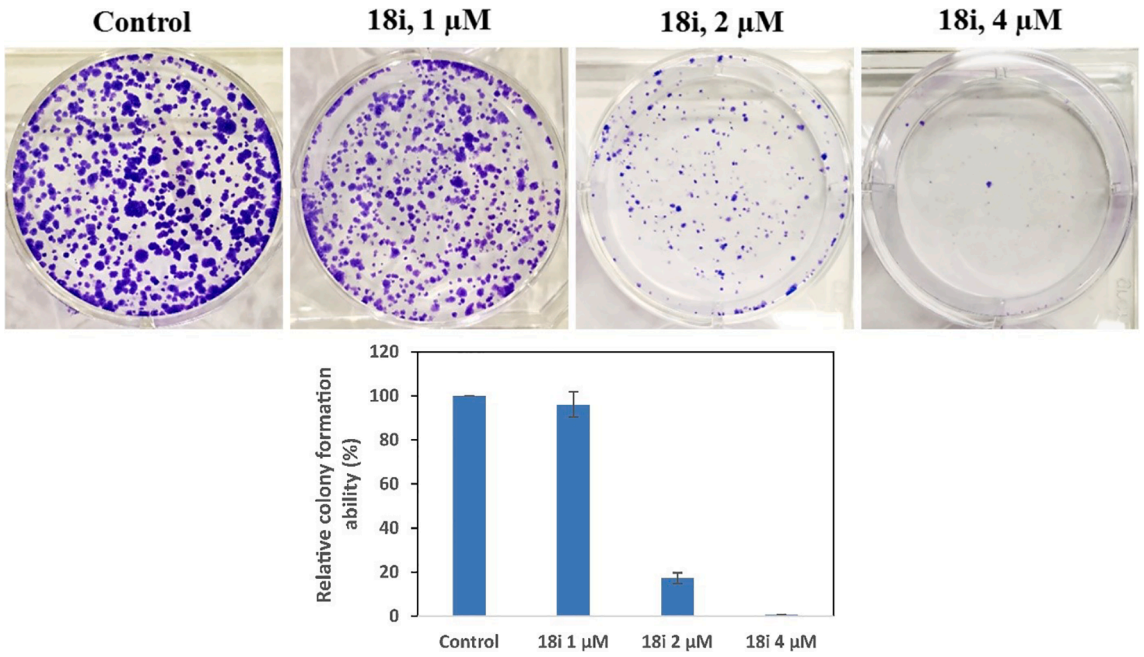

Fig. 10. Colony formation inhibition effect of compound **18i** on A549 cells..

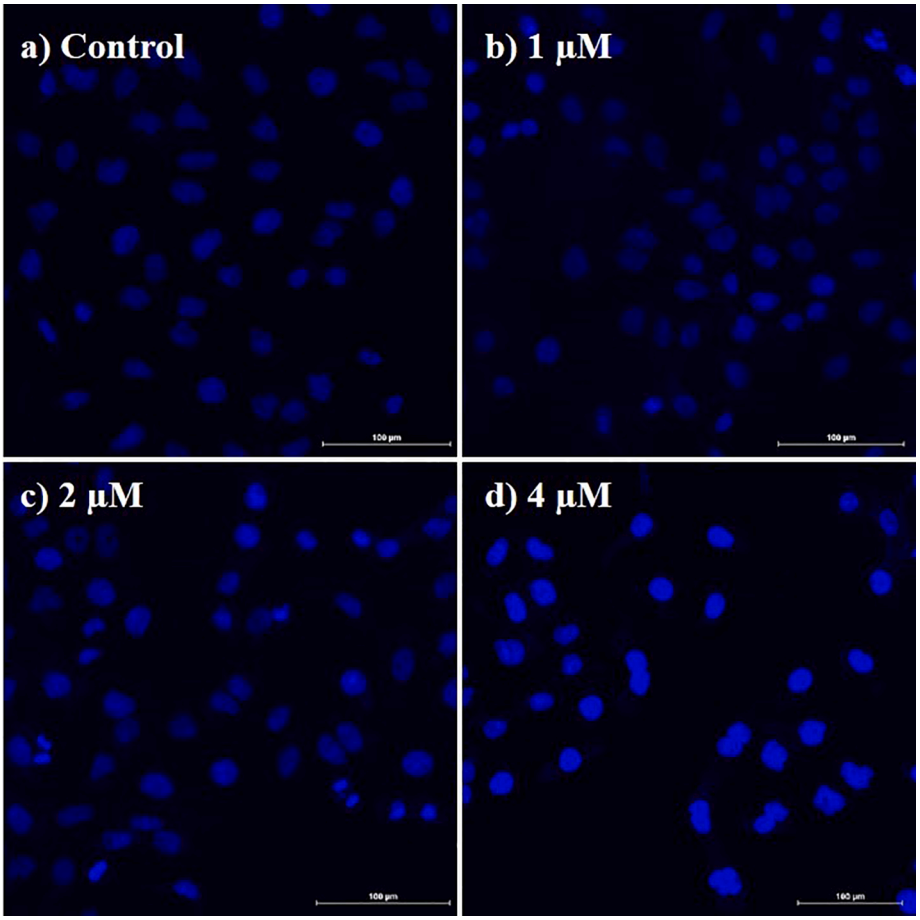

Fig. 11. Apoptosis induced by compound **18i** in A549 cells, observed by fluorescence microscopy using Hoechst 33242 staining after 48 h. The cells were assessed for morphological changes, such as chromatin condensation and nuclear fragmentation, which are hallmarks of cell apoptosis. Scale bar represents 100 μm.

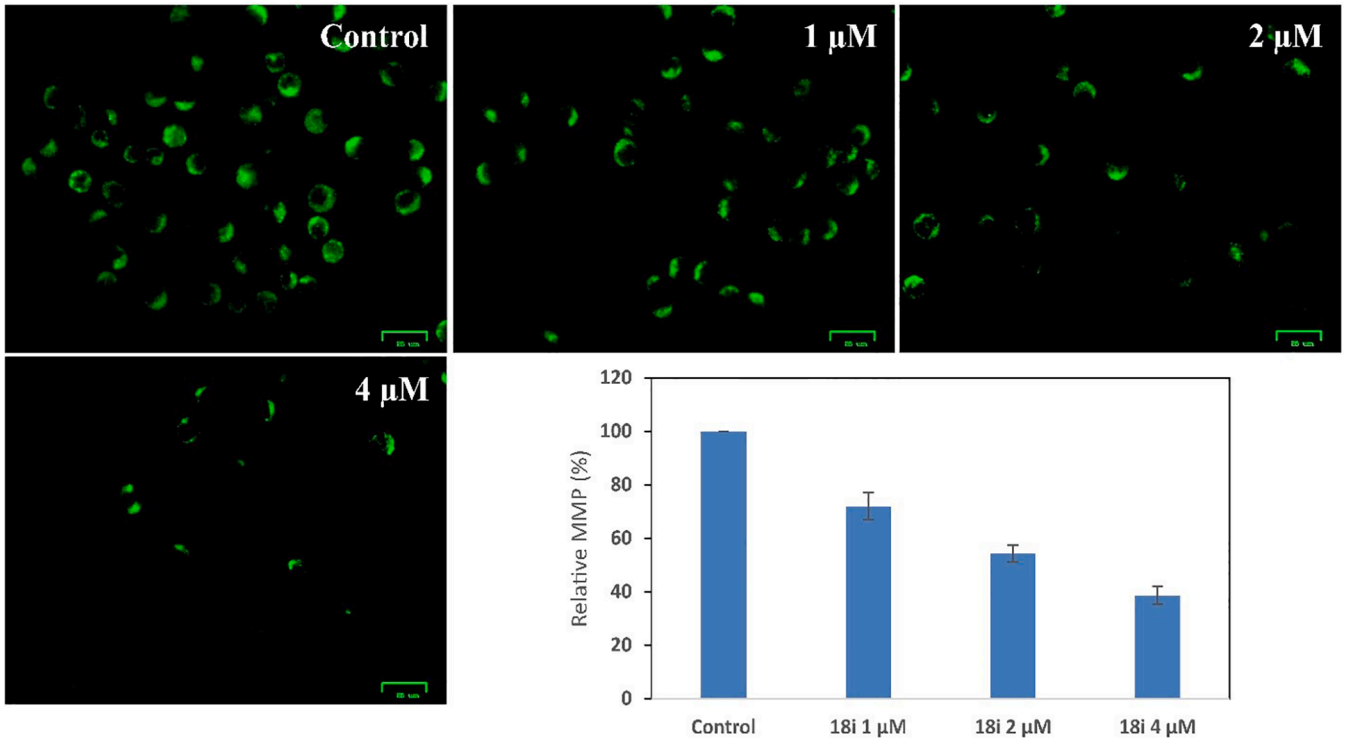

Fig. 12. Compound **18i** disrupted mitochondrial membrane integrity. A549 cells were treated with 1, 2 and 4 µM concentrations of compound **18i** for 48 h, stained with rhodamine123 and imaged by fluorescence microscopy. Scale bar represents 25 µm.

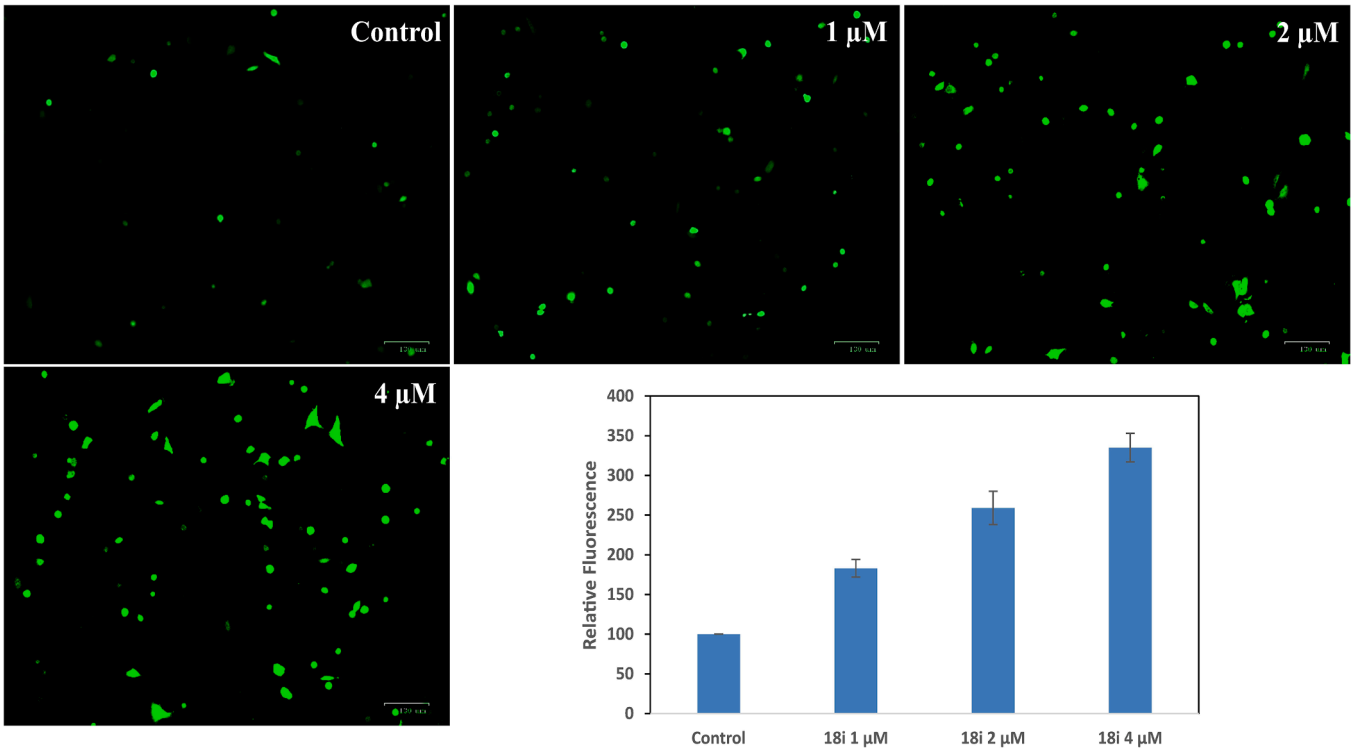

Fig. 13. Compound **18i** induced production of intracellular ROS in A549 cancer cells. Cells were treated with increasing concentration of compound **18i** for 48 h and stained with 10 µM DCFDA. Images were captured by a fluorescence microscope. Scale bar represents 100 µm.

*7.1.1. Synthesis of 4-chloro-6-(piperazin-1-yl)pyrimidin-2-amine **13***

To a solution of 4,6-dichloropyrimidin-2-amine (**11**, 1 mmol) in acetonitrile (3 mL), piperazine (**12**, 6 mmol) was added followed by the addition of potassium carbonate (2 mmol). The resulting mixture was then refluxed at 80 °C for 0.5 h. Upon completion of the reaction as monitored by TLC, acteonitrile was evaporated and the crude compound

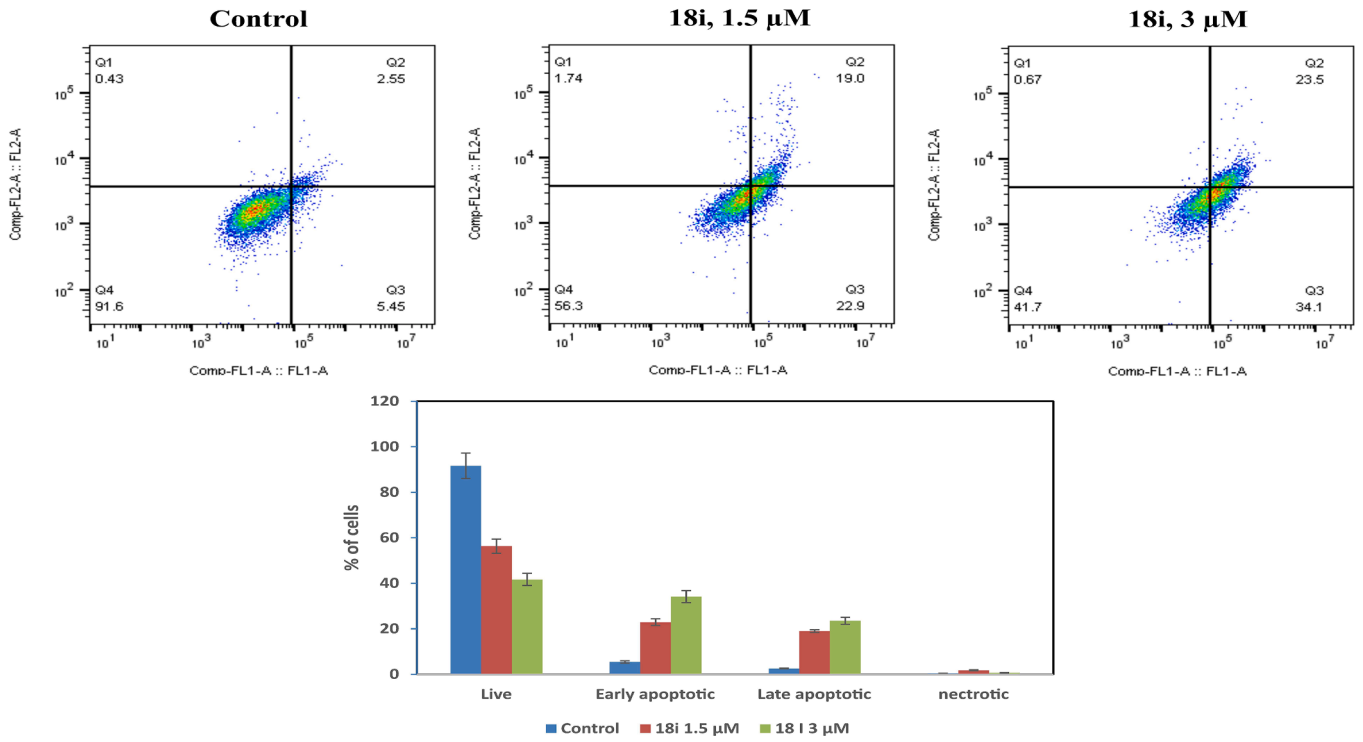

Fig. 14. Analysis of apoptotic cells induced by compound **18i** by flow cytometry. A549 cells exposed to increasing concentrations of compound **18i** (1.5 and 3 µM) were stained with Annexin V-FITC and PI. (Q4: live; Q3: early apoptotic; Q2: late apoptotic; Q1: necrotic). The flow cytometry data analysed by FlowJo software.

was extracted using ethyl acetate as a solvent, to obtain free solid of the corresponding product **13**.

*7.1.2. Synthesis of 4-((5-substituted-1H-benzo[d]imidazol-2-yl)thio)-6-(piperazin-1-yl)pyrimidin-2-amine (**14a-c**)*

To a solution of 4-chloro-6-(piperazin-1-yl)pyrimidin-2-amine (**13**, 1 mmol) and 5-substituted-1*H*-benzo[*d*]imidazole-2-thiol (**3a-c**, 0.75 mmol) and in ethanol, methane sulfonic acid (5 mL) was added slowly. The resulting reaction mixture was refluxed under nitrogen atmosphere for 12 h. Upon completion of the reaction as monitored by TLC, ethanol was evaporated. The crude product obtained was dissolved in ethyl acetate and extracted using $NaHCO_3$ solution. The compound was crystallized using methanol and *tert*-butyl methyl ether (2:8) as a solvent, to obtain free solid of the corresponding product **14a-c**.

*7.1.3. Synthesis of N^4-(2-substituted-1H-benzo[d]imidazol-6-yl)-6-(piperazin-1-yl)pyrimidine-2,4-diamine (**15a,b**)*

To a solution of 4-chloro-6-(piperazin-1-yl)pyrimidin-2-amine (**13**, 1 mmol) and 5-amino-2-phenyl-1*H*-benzo[*d*]imidazole (**7a**,**b**, 0.75 mmol) and in butanol, conc.HCl (5 mL) was added slowly. The resulting reaction mixture was refluxed at 80 °C for 12 h. Upon completion of the reaction as monitored by TLC, ethanol was evaporated. The crude product obtained was dissolved in ethyl acetate and extracted using $NaHCO_3$ solution. The compound was crystallized using methanol and *tert*-butyl methyl ether (2:8) as a solvent, to obtain a free solid of the corresponding product **15a**,**b**.

*7.1.4. Synthesis of new hybrids **17a-u** and **18a-j***

To a mixture of thio and amine derivatives (**14a-c** and **15a**,**b**, 1 equiv.), substituted cinnamic acids (**16a-k**, 1 equiv.), in DMF, EDC (2 equiv.) was added and stirred at 25 °C till complete consumption of the starting materials as determined by TLC. The reaction mixture was then quenched with ice-cold water and extracted using ethyl acetate (3 × 25 mL). The organic layer was concentrated under *in vacuo* and the residue obtained was chromatographed on silica gel (elution with hexane/EtOAc = 6:4–4:6) to provide the hybrids **17a-u** and **18a-j** in moderate to good yields.

*7.1.4.1. (E)-1-(4-(6-((1H-Benzo[d]imidazol-2-yl)thio)-2-aminopyrimidin-4-yl)piperazin-1-yl)-3-phenylprop-2-en-1-one (**17a**).* White solid; yield 83%; mp: 160–164 °C; FT-IR (cm^{-1}): 3365, 3116, 2922, 2862, 1897, 1710, 1370, 738; ^{1}H NMR (500 MHz, DMSO-d_6): δ 13.07 (s, 1H), 7.73 (d, J = 6.8 Hz, 2H), 7.60 (d, J = 3.9 Hz, 2H), 7.52 (d, J = 15.4 Hz, 1H), 7.44–7.38 (m, 3H), 7.28 (d, J = 15.4 Hz, 1H), 7.25–7.20 (m, 2H), 6.55 (s, 2H), 6.10 (s, 1H), 3.80–3.55 (m, 8H); ^{13}C NMR (125 MHz, DMSO-d_6): δ 165.1, 162.3, 161.5, 143.9, 142.2, 139.1, 135.5, 130.0, 129.2, 128.5, 122.9, 118.5, 115.3, 91.2, 44.9, 44.3, 43.7, 41.7; HRMS (ESI): *m/z* calculated for $C_{24}H_{24}N_7OS$ 458.1763 found 458.17682 $[M + H]^+$.

*7.1.4.2. (E)-1-(4-(6-((1H-Benzo[d]imidazol-2-yl)thio)-2-aminopyrimidin-4-yl)piperazin-1-yl)-3-(2,6-dimethoxyphenyl)prop-2-en-1-one (**17b**).* Off-white solid; yield 80%; mp:161–165 °C; FT-IR (cm^{-1}): 3325, 3062, 1650, 1585, 780, 710; ^{1}H NMR (500 MHz, DMSO-d_6): δ 13.19 (s, 1H), 7.87–7.74 (m, 1H), 7.66–7.52 (m, 2H), 7.38 (d, J = 2.7 Hz, 1H), 7.29–7.13 (m, 3H), 7.07–6.91 (m, 2H), 6.55 (s, 2H), 6.18–6.00 (m, 1H), 3.84 (s, 1H), 3.78 (d, J = 16.8 Hz, 3H), 3.73–3.47 (m, 8H); ^{13}C NMR (125 MHz, DMSO-d_6): δ 165.3, 164.5, 162.5, 162.5, 153.6, 152.3, 144.2, 136.5, 124.5, 122.6, 118.5, 116.9, 113.2, 113.1, 89.9, 56.5, 56.1, 45.4, 43.6, 43.5, 41.8; HRMS (ESI): *m/z* calculated for $C_{26}H_{28}N_7O_3S$ 518.1974 found 518.1990 $[M + H]^+$.

*7.1.4.3. (E)-1-(4-(6-((1H-Benzo[d]imidazol-2-yl)thio)-2-aminopyrimidin-4-yl)piperazin-1-yl)-3-(3,4,5-trimethoxyphenyl)prop-2-en-1-one (**17c**).* Off-white solid; yield 83%; mp:158–161 °C; FT-IR (cm^{-1}): 3325, 3062, 1650, 1585, 780, 710; ^{1}H NMR (500 MHz, DMSO-d_6): δ 13.18 (s, 1H), 7.82–7.78 (m, 1H), 7.58–7.41 (m, 2H), 7.22 (d, J = 2.7 Hz, 1H), 7.19–7.00 (m, 2H), 6.98–6.94 (m, 2H), 6.54 (s, 2H), 6.17–6.02 (m, 1H), 3.83 (d, J = 16.8 Hz, 6H), 3.75–3.55 (m, 8H); ^{13}C NMR (125 MHz, DMSO-d_6): δ 164.6 , 163.8, 161.9, 161.8, 153.0, 151.6, 143.6, 135.9, 123.8, 122.0, 117.9, 116.2, 112.6, 112.4, 89.3, 55.9, 55.4, 44.1, 43.9,

40.9; HRMS (ESI): *m/z* calculated for $C_{27}H_{30}N_7O_4S$ 548.2080 found 548.2108 $[M + H]^+$.

7.1.4.4. (E)-1-(4-(6-((1H-Benzo[d]imidazol-2-yl)thio)-2-amino-pyrimidin-4-yl)piperazin-1-yl)-3-(3,4-dihydroxyphenyl)prop-2-en-1-one ***(17d)***. Light-brown solid; yield 72%; mp:163–167 °C; FT-IR (cm^{-1}): 3372, 3112, 2927, 2856, 1839, 1788, 1367, 748; ^1H NMR (500 MHz, DMSO-d_6): δ 13.05 (s, 1H), 9.44 (s, 1H), 9.04 (d, $J = 8.2$ Hz, 1H), 7.59 (s, 2H), 7.35 (d, $J = 14.9$ Hz, 1H), 7.23 (s, 2H), 7.10 (s, 1H), 7.06–6.85 (m, 2H), 6.76 (s, 1H), 6.53 (s, 2H), 6.08 (s, 1H), 3.66–3.54 (m, 8H); ^{13}C NMR (125 MHz, DMSO-d_6): δ 165.1, 162.3, 161.5, 143.9, 142.2, 139.1, 135.5, 130.0, 129.2, 128.5, 122.9, 118.5, 115.3, 91.2, 44.8, 44.3, 43.5, 41.7; HRMS (ESI): *m/z* calculated for $C_{24}H_{24}N_7O_3S$ 490.1661 found 490.1695 $[M + H]^+$.

7.1.4.5. (E)-1-(4-(6-((1H-Benzo[d]imidazol-2-yl)thio)-2-amino-pyrimidin-4-yl)piperazin-1-yl)-3-(3-hydroxy-4-methoxyphenyl)prop-2-en-1-one ***(17e)***. Off-white solid; yield 74%; mp:179–183 °C; FT-IR (cm^{-1}): 3376, 3115, 2949, 2832, 1837, 1768, 1347, 774; ^1H NMR (500 MHz, DMSO-d_6): δ 13.06 (s, 1H), 9.43 (s, 1H), 7.60 (s, 2H), 7.44 (d, $J = 15.1$ Hz, 1H), 7.33 (s, 1H), 7.23 (s, 2H), 7.16–7.02 (m, 2H), 6.78 (s, 1H), 6.54 (s, 2H), 6.08 (s, 1H), 3.83 (s, 3H), 3.76–3.51 (m, 8H); ^{13}C NMR (125 MHz, DMSO-d_6): δ 165.4, 164.5, 162.5, 162.5, 157.3, 144.3, 137.1, 131.5, 128.8, 123.9, 122.5, 120.9, 118.4, 112.9, 90.0, 64.1, 44.9, 44.0, 43.6, 41.6. HRMS (ESI): *m/z* calculated for $C_{25}H_{26}N_7O_3S$ 504.1818 found 504.1840 $[M + H]^+$.

7.1.4.6. (E)-1-(4-(6-((1H-Benzo[d]imidazol-2-yl)thio)-2-amino-pyrimidin-4-yl)piperazin-1-yl)-3-(2-bromo-4,6-dimethoxyphenyl)prop-2-en-1-one ***(17f)***. Brown solid; yield 85%; mp:165–168 °C; FT-IR (cm^{-1}): 3372, 3118, 2949, 2822, 1827, 1799, 1370, 747; ^1H NMR (500 MHz, DMSO-d_6): δ 13.05 (s, 1H), 7.76 (d, $J = 15.2$ Hz, 1H), 7.58 (s, 2H), 7.47 (s, 1H), 7.20 (d, $J = 13.9$ Hz, 4H), 6.54 (s, 2H), 6.06 (s, 1H), 3.87 (d, $J = 4.2$ Hz, 3H), 3.82 (s, 3H), 3.62–3.59 (m, 8H); ^{13}C NMR (125 MHz, DMSO-d_6): δ 165.0, 164.6, 162.5, 151.3, 149.1, 144.2, 140.1, 126.8, 119.1, 116.5, 116.1, 111.1, 90.0, 56.6, 56.5, 44.5, 44.2, 41.3; HRMS (ESI): *m/z* calculated for $C_{26}H_{27}BrN_7O_3S$ 596.1079 found 598.1063 $[M + 2]^+$.

7.1.4.7. (E)-1-(4-(6-((1H-Benzo[d]imidazol-2-yl)thio)-2-amino-pyrimidin-4-yl)piperazin-1-yl)-3-(4-nitrophenyl)prop-2-en-1-one ***(17g)***. Yellow solid; yield 89%; mp:161–165 °C; FT-IR (cm^{-1}): 3366, 3111, 2922, 2853, 1822, 1733, 1398, 762; ^1H NMR (500 MHz, DMSO-d_6): δ 13.06 (s, 1H), 8.25 (d, $J = 6.3$ Hz, 2H), 8.02 (d, $J = 8.8$ Hz, 2H), 7.58 (dd, $J = 6.3$, 7.7 Hz, 4H), 7.23 (s, 2H), 6.55 (s, 2H), 6.13 (s, 1H), 3.79 (s, 2H), 3.63–3.57 (m, 6H); ^{13}C NMR (125 MHz, DMSO-d_6): δ 164.6, 164.5, 162.5, 148.0, 144.3, 142.2, 139.6, 129.8, 129.5, 124.3, 124.2, 123.2, 122.7, 90.0, 45.0, 44.5, 43.5, 42.0; HRMS (ESI): *m/z* calculated for $C_{24}H_{23}N_8O_3S$ 503.1614 found 503.1642 $[M + H]^+$.

7.1.4.8. (E)-1-(4-(2-amino-6-((5-methoxy-1H-benzo[d]imidazol-2-yl) thio)pyrimidin-4-yl)piperazin-1-yl)-3-phenylprop-2-en-1-one ***(17h)***. Off-white solid; yield 75%; mp:159–163 °C; FT-IR (cm^{-1}): 3369, 3119, 2982, 2843, 1838, 1892, 1489, 742; ^1H NMR (500 MHz, DMSO-d_6): δ 12.92 (s, 1H), 7.99 (d, $J = 8.4$ Hz, 1H), 7.58–7.52 (m, 1H), 7.48 (s, 1H), 7.45–7.39 (m, 1H), 7.35 (t, $J = 7.5$ Hz, 1H), 7.23 (d, $J = 15.5$ Hz, 1H), 7.06 (d, $J = 8.2$ Hz, 2H), 6.97 (t, $J = 7.4$ Hz, 1H), 6.86 (d, $J = 7.4$ Hz, 1H), 6.50 (s, 2H), 6.00 (s, 1H), 3.80 (s, 3H), 3.76–3.51 (m, 8H); ^{13}C NMR (125 MHz, DMSO-d_6): δ 165.3, 165.0, 165.0, 162.5, 142.2, 142.0, 135.5, 130.0, 129.2, 129.1, 128.5, 128.4, 118.6, 113.4, 89.6, 55.9, 44.8, 44.1, 43.5, 41.5; HRMS (ESI): *m/z* calculated for $C_{25}H_{26}N_7O_2S$ 488.1869 found 488.1898 $[M + H]^+$.

7.1.4.9. (E)-1-(4-(2-Amino-6-((5-methoxy-1H-benzo[d]imidazol-2-yl) thio)pyrimidin-4-yl)piperazin-1-yl)-3-(2-ethoxyphenyl)prop-2-en-1-one ***(17i)***. White solid; yield 83%; mp:198–202 °C; FT-IR (cm^{-1}): 3372, 3118, 2922, 2853, 1832, 1793, 1389, 752; ^1H NMR (500 MHz, DMSO-d_6): δ 12.92 (s, 1H), 7.78 (dd, $J = 7.4$, 5.2 Hz, 2H), 7.51 (d, $J = 9.9$ Hz, 1H), 7.35 (s, 1H), 7.23 (d, $J = 5.1$ Hz, 1H), 7.05 (d, $J = 7.0$ Hz, 2H), 6.97 (s, 1H), 6.86 (s, 1H), 6.50 (s, 2H), 5.99 (s, 1H), 4.11 (d, $J = 5.9$ Hz, 2H), 3.80 (s, 3H), 3.74–3.40 (m, 8H), 1.39 (s, 3H); ^{13}C NMR (125 MHz, DMSO-d_6): δ 172.5, 165.2, 163.5, 163.4, 153.5, 142.6, 139.3, 131.1, 130.7, 130.0, 129.4, 126.6, 117.6, 106.1, 75.5, 60.5, 56.5, 44.9, 44.6, 43.9, 41.4, 21.5; HRMS (ESI): $C_{27}H_{30}N_7O_3S$ 532.2131 found 532.2162 $[M + H]^+$.

7.1.4.10. (E)-1-(4-(2-Amino-6-((5-methoxy-1H-benzo[d]imidazol-2-yl) thio)pyrimidin-4-yl)piperazin-1-yl)-3-(2,6-dimethoxyphenyl)prop-2-en-1-one ***(17j)***. White solid; yield 72%; mp:172–176 °C; FT-IR (cm^{-1}): 3370, 3116, 2983, 2868, 1849, 1565, 1368, 848; ^1H NMR (500 MHz, DMSO-d_6): δ 12.93 (s, 1H), 7.75 (d, $J = 8.5$ Hz, 1H), 7.49 (d, $J = 7.7$ Hz, 3H), 7.21 (s, 2H), 7.07 (s, 1H), 6.85 (s, 1H), 6.49 (s, 2H), 5.97 (s, 1H), 3.86 (s, 3H), 3.78 (s, 6H), 3.62–3.56 (m, 8H); ^{13}C NMR (125 MHz, DMSO-d_6): δ 165.3, 165.08, 162.5, 162.4, 156.4, 153.7, 152.3, 136.5, 124.5, 118.6, 116.9, 113.3, 113.1, 112.4, 89.7, 56.7, 56.1, 45.1, 44.3, 41.3, 41.5; HRMS (ESI): *m/z* calculated for $C_{27}H_{30}N_7O_4S$ 548.2080 found 548.2108 $[M + H]^+$.

7.1.4.11. (E)-1-(4-(2-Amino-6-((5-methoxy-1H-benzo[d]imidazol-2-yl) thio)pyrimidin-4-yl)piperazin-1-yl)-3-(3,4,5-trimethoxyphenyl)prop-2-en-1-one ***(17k)***. White solid; yield 89%; mp:170–173 °C; FT-IR (cm^{-1}): 3378, 3119, 2973, 2853, 1839, 1614, 1368, 748; ^1H NMR (500 MHz, DMSO-d_6): δ 12.93 (s, 1H), 7.80 (d, $J = 8.5$ Hz, 1H), 7.49 (s, 1H), 7.37 (s, 1H), 7.23 (s, 1H), 7.07 (s, 1H), 6.99 (s, 1H), 6.85 (s, 1H), 6.49 (s, 2H), 5.98 (s, 1H), 3.78 (d, $J = 7.6$ Hz, 12H), 3.68–3.37 (m, 8H); ^{13}C NMR (125 MHz, DMSO-d_6): δ 164.6, 164.4, 161.8, 161.8, 155.7, 153.0, 151.6, 135.9, 123.9, 117.9, 116.2, 112.6, 112.4, 111.7, 89.0, 55.8, 55.4, 55.2, 44.4, 43.6, 42.5, 40.7; HRMS (ESI): *m/z* calculated for $C_{28}H_{32}N_7O_5S$ 578.2186 found 578.2210 $[M + H]^+$.

7.1.4.12. (E)-1-(4-(2-Amino-6-((5-methoxy-1H-benzo[d]imidazol-2-yl) thio)pyrimidin-4-yl)piperazin-1-yl)-3-(2-bromo-4,6-dimethoxyphenyl)prop-2-en-1-one ***(17l)***. Off-white solid, yield 85%; mp:185–189 °C; FT-IR (cm^{-1}): 3348, 3012, 2972, 2853, 1864, 1710, 1288, 753; ^1H NMR (500 MHz, DMSO-d_6): δ 12.93 (s, 1H), 7.99 (d, $J = 7.3$ Hz, 1H), 7.75 (d, $J = 7.2$ Hz, 1H), 7.47 (s, 2H), 7.19 (d, $J = 6.7$ Hz, 2H), 7.07 (s, 1H), 6.49 (s, 2H), 5.97 (s, 1H), 3.86 (s, 3H), 3.80 (s, 6H), 3.69–3.42 (m, 8H); ^{13}C NMR (125 MHz, DMSO-d_6): δ 164.2, 163.9, 161.4, 161.3, 155.3, 152.6, 151.2, 135.4, 123.4, 117.4, 115.7, 112.2, 112.0, 111.3, 88.6, 55.1, 54.8, 43.7, 42.9, 42.1, 40.7; HRMS (ESI): *m/z* calculated for $C_{27}H_{29}BrN_7O_4S$ 626.1184 found 628.1170 $[M + 2]^+$.

7.1.4.13. (E)-1-(4-(2-Amino-6-((5-methoxy-1H-benzo[d]imidazol-2-yl) thio)pyrimidin-4-yl)piperazin-1-yl)-3-(4-bromophenyl)prop-2-en-1-one ***(17m)***. Off-white solid; yield 87%; mp: 193–197 °C; FT-IR (cm^{-1}): 3358, 3212, 2976, 2876, 1862, 1712, 1509, 1395, 755; ^1H NMR (500 MHz, DMSO-d_6): δ 12.92 (s, 1H), 7.80 (s, 2H), 7.50 (s, 2H), 7.25 (s, 3H), 7.07 (s, 1H), 6.86 (s, 1H), 6.50 (s, 2H), 5.98 (s, 1H), 3.80–3.53 (m, 11*H*); ^{13}C NMR (125 MHz, DMSO-d_6): δ 165.4, 164.8, 162.8, 162.5, 140.8, 134.9, 132.1, 130.5, 123.2, 119.5, 89.6, 55.9, 44.8, 44.3, 43.6, 41.6; HRMS (ESI): *m/z* calculated for $C_{25}H_{25}BrN_7O_2S$ 566.0974 found 568.0961 $[M + 2]^+$.

7.1.4.14. (E)-1-(4-(2-Amino-6-((5-methoxy-1H-benzo[d]imidazol-2-yl) thio)pyrimidin-4-yl)piperazin-1-yl)-3-(4-nitrophenyl)prop-2-en-1-one ***(17n)***. Yellow solid; yield 76%; mp: 195–198 °C; FT-IR (cm^{-1}): 3368, 3112, 2967, 2886, 1878, 1705, 1619, 1385, 765; ^1H NMR (500 MHz, DMSO-d_6): δ 12.91 (s, 1H), 7.42 (s, 2H), 7.32 (s, 1H), 7.06 (t, $J = 21.7$ Hz, 3H), 6.80 (d, $J = 49.4$ Hz, 3H), 6.51 (d, $J = 17.9$ Hz, 2H), 5.97 (s, 1H), 3.80 (s, 3H), 3.62 (d, $J = 91.9$ Hz, 8H); ^{13}C NMR (125 MHz,

DMSO-d_6): δ 164.5, 157.5, 148.0, 142.1, 140.3, 139.8, 137.1, 131.8, 129.6, 124.3, 123.0, 116.4, 114.5, 97.0, 56.2, 44.6, 41.8.; HRMS (ESI): *m/z* calculated for $C_{25}H_{25}N_8O_4S$ 533.1719 found 533.1754 $[M + H]^+$.

7.1.4.15. (E)-1-(4-(2-Amino-6-((5-(difluoromethoxy)-1H-benzo[d]imidazol-2-yl)thio)pyrimidin-4-yl)piperazin-1-yl)-3-phenylprop-2-en-1-one ***(17o)***. Off-white solid; yield 84%; mp:160–164 °C; FT-IR (cm − 1): 3325, 3062, 2887, 1650, 1585, 780, 710; ^{1}H NMR (500 MHz, DMSO-d_6): δ 13.20 (s, 1H), 7.73 (d, *J* = 7.1 Hz, 2H), 7.61 (d, *J* = 8.4 Hz, 1H), 7.53 (d, *J* = 15.4 Hz, 1H), 7.44–7.36 (m, 4H), 7.34–7.15 (m, 2H), 7.07 (d, *J* = 10.8 Hz, 1H), 6.57 (s, 2H), 6.15 (s, 1H), 3.78–3.57 (m, 8H); ^{13}C NMR (125 MHz, DMSO- d_6): δ 165.1, 164.0, 162.9, 162.5, 142.2, 135.5, 130.0, 129.2, 128.5, 128.1, 119.3, 118.8, 118.6, 117.3, 115.3, 90.2, 44.2, 43.8, 43.4, 41.5; HRMS (ESI): *m/z* calculated for $C_{25}H_{24}F_2N_7O_2S$ 524.1680 found 524.1699 $[M + H]^+$.

7.1.4.16. (E)-1-(4-(2-Amino-6-((5-(difluoromethoxy)-1H-benzo[d]imidazol-2-yl)thio)pyrimidin-4-yl)piperazin-1-yl)-3-(2-ethoxyphenyl)prop-2-en-1-one ***(17p)***. Off-white solid; yield 80%; mp:162–165 °C; FT-IR (cm^{-1}): 3325, 3062, 2767, 1650, 1585, 780, 710; ^{1}H NMR (500 MHz, DMSO-d_6): δ 13.20 (s, 1H), 7.79 (dd, *J* = 20.6, 11.5 Hz, 2H), 7.61 (d, *J* = 7.9 Hz, 1H), 7.37 (dd, *J* = 17.3, 11.1 Hz, 2H), 7.24 (d, *J* = 15.5 Hz, 1H), 7.17–6.98 (m, 3H), 6.98 (t, *J* = 7.4 Hz, 1H), 6.57 (s, 2H), 6.15 (s, 1H), 4.11 (dd, *J* = 13.7, 6.8 Hz, 2H), 3.76–3.55 (m, 8H), 1.38 (s, 3H); ^{13}C NMR (125 MHz, DMSO-d_6): 165.4, 164.2, 162.5, 157.3, 137.1, 131.5, 128.8, 123.9, 120.9, 119.5, 118.4, 117.3, 115.3, 112.9, 90.2, 64.1, 44.9, 44.3, 43.6, 41.5, 15.1; HRMS (ESI): *m/z* calculated for $C_{27}H_{28}F_2N_7O_3S$ 568.1942 found 568.1978 $[M + H]^+$.

7.1.4.17. (E)-1-(4-(2-Amino-6-((5-(difluoromethoxy)-1H-benzo[d]imidazol-2-yl)thio)pyrimidin-4-yl)piperazin-1-yl)-3-(2,6-dimethoxyphenyl)prop-2-en-1-one ***(17q)***. Off-white solid; yield 80%; mp:161–164 °C; FT-IR (cm^{-1}): 3325, 3262, 2898,1650, 1585, 780, 710; ^{1}H NMR (500 MHz, DMSO-d_6): δ 13.20 (s, 1H), 7.80 (d, *J* = 15.5 Hz, 1H), 7.61 (d, *J* = 8.1 Hz, 1H), 7.39 (d, *J* = 7.9 Hz, 2H), 7.23 (d, *J* = 14.6 Hz, 1H), 7.07 (d, *J* = 9.4 Hz, 1H), 6.99 (d, *J* = 10.2 Hz, 2H), 6.86 (s, 1H), 6.58 (s, 2H), 6.14 (s, 1H), 3.79 (d, *J* = 17.1 Hz, 6H), 3.61 (d, *J* = 27.9 Hz, 8H); ^{13}C NMR (125 MHz, DMSO-d_6): δ 165.3, 163.7, 162.5, 153.7, 152.3, 137.9, 136.5, 124.6, 119.3, 118.6, 117.3, 116.9, 115.2, 114.4, 113.3, 113.2, 90.2, 56.5, 56.1, 46.1, 44.9, 41.7; HRMS (ESI): *m/z* calculated for $C_{27}H_{28}F_2N_7O_4S$ 584.1892 found 584.1924 $[M + H]^+$.

7.1.4.18. (E)-1-(4-(2-Amino-6-((5-(difluoromethoxy)-1H-benzo[d]imidazol-2-yl)thio)pyrimidin-4-yl)piperazin-1-yl)-3-(3,4,5-trimethoxyphenyl) prop-2-en-1-one ***(17r)***. Light brown solid; yield 78%; mp: 188–191 °C; FT-IR (cm^{-1}): 3367, 3114, 2898, 2609, 1859, 1563, 1394, 1275, 785; ^{1}H NMR (500 MHz, DMSO-d_6): δ 13.20 (s, 1H), 7.80 (d, *J* = 15.5 Hz, 1H), 7.61 (d, *J* = 8.1 Hz, 1H), 7.39 (d, *J* = 7.9 Hz, 2H), 7.23 (d, *J* = 14.6 Hz, 1H), 7.07 (d, *J* = 9.4 Hz, 1H), 6.99 (d, *J* = 10.2 Hz, 2H), 6.58 (s, 2H), 6.14 (s, 1H), 3.79–3.65 (m, 9H), 3.64–3.55 (m, 8H); ^{13}C NMR (125 MHz, DMSO-d_6): δ 165.2, 162.5, 159.7, 153.5, 147.5, 142.6, 139.4, 131.1, 119.3, 117.6, 117.6, 117.3, 115.2, 106.2, 91.2, 90.2, 60.5, 56.5, 44.5, 41.5; HRMS (ESI): *m/z* calculated for $C_{28}H_{30}F_2N_7O_5S$ 614.1997 found 614.2024 $[M + H]^+$.

7.1.4.19. (E)-1-(4-(2-Amino-6-((5-(difluoromethoxy)-1H-benzo[d]imidazol-2-yl)thio)pyrimidin-4-yl)piperazin-1-yl)-3-(3,4,5-trimethoxyphenyl) prop-2-en-1-one ***(17s)***. Light brown solid; yield 72%; mp: 183–187 °C; FT-IR (cm^{-1}): 3368, 3112, 2920, 2651, 1851, 1556, 1389, 1285, 760; ^{1}H NMR (500 MHz, DMSO-d_6): δ 13.08 (s, 1H), 7.82 (s, 2H), 7.72 (d, *J* = 8.0 Hz, 4H), 7.58 (d, *J* = 15.3 Hz, 3H), 7.49 (t, *J* = 7.6 Hz, 2H), 7.40 (t, *J* = 7.3 Hz, 1H), 7.33 (d, *J* = 15.4 Hz, 1H), 7.23 (s, 2H), 6.56 (s, 2H), 6.11 (s, 1H), 3.79 (s, 2H), 3.60 (d, *J* = 27.8 Hz, 6H); ^{13}C NMR (125 MHz, DMSO-d_6): δ 165.1, 164.6, 162.5, 162.5, 144.3, 141.7, 141.6, 139.8, 134.7, 129.4, 129.2, 128.3, 127.4, 127.1, 118.5, 89.9, 44.6, 44.4, 43.4, 41.5; HRMS (ESI): *m/z* calculated for $C_{31}H_{28}F_2N_7O_2S$ 600.1993 found 600.2028 $[M + H]^+$.

7.1.4.20. (E)-3-([1,1′-Biphenyl]-4-yl)-1-(4-(2-amino-6-((5-(difluoromethoxy)-1H-benzo[d]imidazol-2-yl)thio)pyrimidin-4-yl)piperazin-1-yl) prop-2-en-1-one ***(17t)***. White solid; yield 88%; mp: 192–196 °C; FT-IR (cm^{-1}): 3346, 3119, 2986, 1689, 1654, 1527, 1203, 875; ^{1}H NMR (500 MHz, DMSO-d_6): δ 13.20 (s, 1H), 7.76 (d, *J* = 15.2 Hz, 1H), 7.61 (d, *J* = 8.2 Hz, 1H), 7.48 (s, 1H), 7.38 (dd, *J* = 25.7, 7.3 Hz, 2H), 7.21 (dd, *J* = 10.8, 4.1 Hz, 2H), 7.07 (d, *J* = 10.5 Hz, 1H), 6.56 (s, 2H), 6.13 (s, 1H), 3.87 (s, 3H), 3.82 (s, 3H), 3.68–3,56 (m, 8H); ^{13}C NMR (125 MHz, DMSO-d_6): δ 165.2, 164.9, 164.0, 162.5, 151.3, 149.0, 140.1, 126.8, 119.6, 119.1, 117.3, 116.5, 116.0, 115.3, 115.1, 111.0, 90.1, 56.6, 56.5, 45.3, 45.1, 43.1; HRMS (ESI): *m/z* calculated for $C_{27}H_{27}BrF_2N_7O_4S$ 662.0997 found 664.0980 $[M + 2]^+$.

7.1.4.21. (E)-1-(4-(2-Amino-6-((5-(difluoromethoxy)-1H-benzo[d]imidazol-2-yl)thio)pyrimidin-4-yl)piperazin-1-yl)-3-(4-bromophenyl)prop-2-en-1-one ***(17u)***. Off-white solid; yield 85%; mp: 190–194 °C; FT-IR (cm^{-1}): 3369, 3285, 2981, 1695, 1656, 1635, 1253, 831; ^{1}H NMR (500 MHz, DMSO-d_6): δ 13.21 (s, 1H), 7.71 (d, *J* = 8.0 Hz, 2H), 7.62 (d, *J* = 7.9 Hz, 3H), 7.49 (d, *J* = 15.3 Hz, 1H), 7.36 (dd, *J* = 24.5, 17.1 Hz, 2H), 7.21 (s, 1H), 7.08 (d, *J* = 10.3 Hz, 1H), 6.57 (s, 2H), 6.15 (s, 1H), 3.85–3.57 (m, 8H); ^{13}C NMR (125 MHz, DMSO-d_6): δ 164.3, 163.3, 162.2, 161.8, 141.4, 134.8, 129.3, 128.4, 127.7, 127.4, 118.6, 118.0, 117.9, 116.6, 114.5, 89.4, 43.5, 43.1, 42.6, 40.8; HRMS (ESI): *m/z* calculated for $C_{25}H_{23}BrF_2N_7O_2S$ 602.0785 found 604.0871 $[M + 2]^+$.

7.1.4.22. (E)-1-(4-(2-Amino-6-((2-phenyl-1H-benzo[d]imidazol-5-yl) amino)pyrimidin-4-yl)piperazin-1-yl)-3-(4-methoxyphenyl)prop-2-en-1-one ***(18a)***. Off-white solid; yield 78%; mp: 198–201 °C; FT-IR (cm^{-1}): 3367, 3251, 2891, 1692, 1675, 1643, 1425, 865; ^{1}H NMR (500 MHz, DMSO-d_6): δ 12.66 (s, 1H), 8.67 (s, 1H), 8.21–8.10 (m, 2H), 7.70 (dd, *J* = 11.7, 8.0, Hz, 3H), 7.56–7.45 (m, 5H), 7.31 (dd, *J* = 11.9, 7.6 Hz, 1H), 7.15–7.11 (m, 1H), 6.98 (d, *J* = 8.4 Hz, 2H), 5.77 (s, 2H), 5.42 (s, 1H), 3.81 (s, 3H), 3.77–3.42 (m, 8H); ^{13}C NMR (125 MHz, DMSO-d_6): δ 165.1, 163.8, 163.0, 160.0, 143.1, 142.2, 142.1, 130.0, 129.4, 129.2, 128.5, 128.5, 127.7, 126.7, 124.9, 110.0, 91.3, 62.8, 44.9, 44.1, 41.4; HRMS (ESI): *m/z* calculated for $C_{31}H_{31}N_8O_2$ 547.2570 found 547.2560 $[M + H]^+$.

7.1.4.23. (E)-1-(4-(2-Amino-6-((2-phenyl-1H-benzo[d]imidazol-5-yl) amino)pyrimidin-4-yl)piperazin-1-yl)-3-(3,4,5-trimethoxyphenyl)prop-2-en-1-one ***(18b)***. White solid; yield 86%; mp: 196–199 °C; FT-IR (cm^{-1}): 3368, 3112, 2889, 1698, 1675, 1638, 1412, 890; ^{1}H NMR (500 MHz, DMSO-d_6): δ 12.69 (s, 1H), 8.73 (s, 1H), 8.16 (d, *J* = 7.5 Hz, 2H), 7.85 (s, 1H), 7.54 (t, *J* = 7.5 Hz, 2H), 7.51–7.44 (m, 3H), 7.31 (d, *J* = 8.3 Hz, 1H), 7.20 (d, *J* = 15.3 Hz, 1H), 7.06 (s, 2H), 5.91 (s, 2H), 5.43 (s, 1H), 3.86 (d, *J* = 13.5 Hz, 9H), 3.53 (s, 8H).; ^{13}C NMR (125 MHz, DMSO-d_6): δ 172.3, 165.2, 163.7, 153.5, 153.0, 142.5, 139.5, 131.1, 130.8, 129.9, 129.3, 126.6, 117.7, 106.2, 75.8, 60.5, 56.4, 44.6, 43.3; HRMS (ESI): *m/z* calculated for $C_{33}H_{35}N_8O_4$ 607.2781 found 607.2810 $[M + H]^+$.

7.1.4.24. (E)-1-(4-(2-Amino-6-((2-phenyl-1H-benzo[d]imidazol-5-yl) amino)pyrimidin-4-yl)piperazin-1-yl)-3-(2-bromo-5-methoxyphenyl)prop-2-en-1-one ***(18c)***. White solid; yield 82%; mp: 199–203 °C; FT-IR (cm^{-1}): 3366, 3217, 2936, 1696, 1685, 1587, 1243, 875; ^{1}H NMR (500 MHz, DMSO-d_6): δ 12.59 (s, 1H), 8.61 (s, 1H), 8.09–8.03 (m, 2H), 7.62 (dd, *J* = 11.7, 8.0 Hz, 3H), 7.60–7.53 (m, 3H), 7.46 (dd, *J* = 11.9, 7.6 Hz, 1H), 7.44 (m, 1H), 7.15–7.11 (m, 1H), 6.90 (d, *J* = 8.4 Hz, 2H), 5.71 (s, 2H), 5.35 (s, 1H), 3.74 (s, 3H), 3.68–3.23 (m, 8H); ^{13}C NMR (125 MHz, DMSO-d_6): δ 165.4, 165.3, 163.8, 163.5, 162.9, 162.9, 161.0, 160.9, 141.9, 130.2, 130.1, 130.1, 129.4, 129.3, 129.3, 116.0, 114.7, 820.7, 45.7, 43.9; HRMS (ESI): *m/z* calculated for $C_{31}H_{30}BrN_8O_2$ 625.1675 found 625.1666 $[M + 2]^+$.

*7.1.4.25. (E)-1-(4-(2-Amino-6-((2-phenyl-1H-benzo[d]imidazol-5-yl) amino)pyrimidin-4-yl)piperazin-1-yl)-3-(4-bromophenyl)prop-2-en-1-one **(18d)***. Off-white solid; yield 85%; mp: 199–202 °C; FT-IR (cm^{-1}): 3374, 3267, 2881, 1732, 1702, 1609, 1485, 855; ^{1}H NMR (500 MHz, DMSO-d_6): δ 12.87 (s, 1H), 9.04 (s, 1H), 8.18 (d, J = 7.2 Hz, 2H), 8.16 (d, J = 8.3 Hz, 1H), 7.73 (s, 3H), 7.55–7.52 (m, 3H), 7.42 (d, J = 7.0 Hz, 3H), 7.29 (d, J = 12.5 Hz, 2H), 6.52 (s, 2H), 6.15 (s, 1H), 3.80–3.56 (m, 8H); ^{13}C NMR (125 MHz, DMSO-d_6): δ 165.1, 163.0, 142.2, 142.1, 135.6, 130.0, 129.4, 129.2, 128.5, 128.5, 127.7, 126.7, 124.9, 119.5, 118.6, 110.0, 91.3, 44.7, 41.4; HRMS (ESI): *m/z* calculated for $C_{30}H_{28}BrN_8O$ 595.1569 found 595.1571 $[M + 2]^+$.

*7.1.4.26. (E)-1-(4-(2-Amino-6-((2-phenyl-1H-benzo[d]imidazol-5-yl) amino)pyrimidin-4-yl)piperazin-1-yl)-3-(4-fluorophenyl)prop-2-en-1-one **(18e)***. White solid; yield 79%; mp: 200–204 °C; FT-IR (cm^{-1}): 3364, 3241, 2781, 1685, 1646, 1427, 1418, 813; ^{1}H NMR (500 MHz, DMSO-d_6): δ 12.81 (s, 1H), 8.99 (s, 1H), 8.12 (d, J = 7.2 Hz, 2H), 7.93 (d, J = 8.3 Hz, 1H), 7.67 (s, 3H), 7.50 (s, 3H), 7.36 (d, J = 7.0 Hz, 3H), 7.23 (d, J = 12.5 Hz, 2H), 6.46 (s, 2H), 6.09 (s, 1H), 3.75–3.50 (m, 8H).; ^{13}C NMR (125 MHz, DMSO-d_6): δ 163.9, 162.3, 161.8, 158.4, 142.2, 141.0, 140.9, 128.8, 128.2, 128.0, 127.3, 127.3, 126.5, 125.5, 123.7, 118.3, 117.4, 108.9, 90.1, 43.5, 43.2, 42.8, 40.3; HRMS (ESI): *m/z* calculated for $C_{30}H_{28}FN_8O$ 535.2370 found 535.2398 $[M + H]^+$.

*7.1.4.27. (E)-1-(4-(2-Amino-6-((2-(trifluoromethyl)-1H-benzo[d]imidazol-5-yl)amino)pyrimidin-4-yl)piperazin-1-yl)-3-phenylprop-2-en-1-one **(18f)***. White solid; yield 73%; mp: 199–201 °C; FT-IR (cm^{-1}): 3364, 3251, 2681, 1675, 1646, 1577, 1428, 871; ^{1}H NMR (500 MHz, DMSO-d_6): δ 13.61 (s, 1H), 8.89 (s, 1H), 8.00 (s, 1H), 7.71 (t, J = 24.8 Hz, 2H), 7.63 (d, J = 14.6 Hz, 1H), 7.54 (d, J = 15.4 Hz, 1H), 7.49 (d, J = 6.6 Hz, 1H), 7.45–7.39 (m, 3H), 7.30 (d, J = 15.4 Hz, 1H), 5.86 (s, 2H), 5.43 (s, 1H), 3.84–3.51 (m, 8H); ^{13}C NMR (125 MHz, DMSO-d_6): δ 165.0, 164.2, 163.7, 162.9, 162.7, 162.2, 140.9, 132.2, 132.2, 130.7, 130.6, 120.7, 118.5, 116.2, 116.0, 76.4, 45.1, 44.4, 43.9, 41.8; HRMS (ESI): *m/z* calculated for $C_{25}H_{24}F_3N_8O$ 509.2025 found 509.2054 $[M + H]^+$.

*7.1.4.28. (E)-1-(4-(2-Amino-6-((2-(trifluoromethyl)-1H-benzo[d]imidazol-5-yl)amino)pyrimidin-4-yl)piperazin-1-yl)-3-(4-methoxyphenyl)prop-2-en-1-one **(18g)***. White solid; yield 76%; mp: 200–204 °C; FT-IR (cm^{-1}): 3364, 3151, 2881, 1685, 1646, 1527, 1418, 813; ^{1}H NMR (500 MHz, DMSO-d_6): δ 13.55 (s, 1H), 8.79 (s, 1H), 7.97 (s, 1H), 7.55 (dd, J = 48.1, 8.1 Hz, 3H), 7.46 (s, 2H), 6.94 (d, J = 7.9 Hz, 3H), 5.77 (s, 2H), 5.38 (s, 1H), 3.77 (s, 3H), 3.58 (dd, J = 78.2, 51.2 Hz, 8H); ^{13}C NMR (125 MHz, DMSO-d_6): 166.1, 163.2, 162.4, 162.2, 158.7, 138.5, 133.3, 120.1, 119.9, 117.9, 116.5, 113.2, 108.4, 75.9, 55.5, 45.6, 43.6, 43.0, 40.7; HRMS (ESI): *m/z* calculated for $C_{26}H_{26}F_3N_8O_2$ 539.2131 found 539.2168 $[M + H]^+$.

*7.1.4.29. (E)-1-(4-(2-Amino-6-((2-(trifluoromethyl)-1H-benzo[d]imidazol-5-yl)amino)pyrimidin-4-yl)piperazin-1-yl)-3-(2,3,4-trimethoxyphenyl) prop-2-en-1-one **(18 h)***. White solid; yield 74%; mp: 199–202 °C; FT-IR (cm^{-1}): 3364, 3271, 2981, 1685, 1666, 1527, 1418, 831; ^{1}H NMR (500 MHz, DMSO-d_6): δ 13.58 (s, 1H), 8.82 (s, 1H), 8.08 (s, 1H), 7.59 (s, 1H), 7.51–7.46 (m, 2H), 7.24–7.19 (m, 1H), 7.06 (s, 2H), 5.82 (s, 2H), 5.44 (s, 1H), 3.85 (s, 9H), 3.53 (s, 8H); ^{13}C NMR (125 MHz, DMSO-d_6): δ 165.2, 163.8, 163.0, 162.9, 153.5, 142.5, 139.4, 131.2, 120.9, 120.5, 118.5, 117.7, 106.2, 76.7, 60.5, 56.6, 49.1, 44.1, 43.7, 41.5; HRMS (ESI): *m/z* calculated for $C_{28}H_{30}F_3N_8O_4$ 599.2342 found 599.2346 $[M + H]^+$.

*7.1.4.30. (E)-1-(4-(2-Amino-6-((2-(trifluoromethyl)-1H-benzo[d]imidazol-5-yl)amino)pyrimidin-4-yl)piperazin-1-yl)-3-(2-bromo-5-methoxyphenyl)prop-2-en-1-one **(18i)***. Light-brown solid; yield 82%; mp: 200–203 °C; FT-IR (cm^{-1}): 3364, 3261, 2881, 1685, 1646, 1527, 1418, 813; ^{1}H NMR (500 MHz, DMSO-d_6): δ 13.57 (s, 1H), 8.82 (s, 1H), 8.00 (s, 1H), 7.52 (dd, J = 48.1, 8.1 Hz, 4H), 6.97 (d, J = 7.9 Hz, 3H), 5.79 (s, 2H), 5.41 (s, 1H), 3.79 (s, 3H), 3.61 (dd, J = 78.2, 51.2 Hz, 8H); ^{13}C NMR (125 MHz, DMSO-d_6): δ 166.7, 163.8, 163.0, 162.8, 159.2, 139.1, 133.9, 120.5, 118.5, 117.1, 113.7, 109.0, 76.5, 56.1, 46.2, 44.2, 43.6; HRMS (ESI): *m/z* calculated for $C_{26}H_{25}BrF_3N_8O_2$ 617.1236 found 617.1221 $[M + 2]^+$.

*7.1.4.31. (E)-1-(4-(2-Amino-6-((2-(trifluoromethyl)-1H-benzo[d]imidazol-5-yl)amino)pyrimidin-4-yl)piperazin-1-yl)-3-(4-fluorophenyl)prop-2-en-1-one **(18j)***. White solid; yield 86%; mp: 195–198 °C; FT-IR (cm^{-1}): 3364, 3251, 2881, 1685, 1546, 1327, 713; ^{1}H NMR (500 MHz, DMSO-d_6): δ 12.75 (s, 1H), 8.66 (s, 1H), 8.16 (s, 2H), 7.71 (s, 1H), 7.61 (s, 1H), 7.53 (d, J = 6.8 Hz, 2H), 7.48 (s, 1H), 7.33 (d, J = 10.8 Hz, 2H), 6.58 (s, 1H), 5.74 (s, 2H), 3.72 (d, J = 63.9 Hz, 4H), 3.48 (d, J = 30.8 Hz, 4H); ^{13}C NMR (125 MHz, DMSO-d_6): δ 164.8, 163.8, 163.4, 163.0, 140.8, 134.9, 132.2, 132.1, 130.8, 130.6, 130.4, 130.1, 129.9, 129.4, 129.3, 129.2, 126.7, 126.6, 123.2, 119.6, 75.9, 45.1, 44.5, 43.8, 41.8; HRMS (ESI): *m/z* calculated for $C_{25}H_{23}F_4N_8O$ 527.1931 found 527.1936 $[M + H]^+$.

7.2. Pharmacology

7.2.1. Cell culture

Prostate (PC-3), lung (A549), Breast (MDAMB-231) and cervical (HeLa) cells were purchased from ATCC and grown in RPMI medium supplemented with 10% fetal bovine serum (FBS) and 1% penicillin–streptomycin (PS). All the cell lines were grown in an incubator with 75% humidity and 5% CO_2 at 37 °C. 0.25% trypsin-ethylenediaminetetraacetic acid (EDTA, Life Technologies) was used for harvesting the cells. For all the assays, stock solutions of the compounds were prepared in DMSO (10 mM). HUVEC cells were grown in M200 medium and 0.05% Trypsin-EDTA was used for detaching the cells from the culture flasks.

7.2.2. Evaluation of in vitro cytotoxic effects

In this assay, prostate (PC-3), lung (A549), Breast (MDA-MB-231) and cervical (HeLa) cells were seeded in 96 well plates depending on their doubling time and were grown overnight. The cells were exposed to different concentrations of cinnamide derivatives of benzimidazole-pyrimidine conjugates **17a-u** & **18a-j** (100, 10, 1, 0.1 and 0.01 μM) for 48 h. Then, the medium containing compounds were removed and replaced with 100 μL of MTT solution (5 mg/mL) and the cells were further incubated for 4 h in dark at 37 °C. The unreacted MTT solution was removed and 100 μL DMSO was added to each well to solubilize the produced formazan crystals. The absorbance of the purple formazan solution was recorded using a plate reader (SpectraMax) at 570 nm and the IC_{50} values for each compound were calculated. All the experiments were repeated three times and the standard deviations are reported in Table 1.

7.2.3. Effect of **18i** on tubulin polymerization inhibition

Tubulin polymerization kit was procured from cytoskeleton, Inc. (BK011). To study the effect of compound **18i**, fluorescence based *in vitro* tubulin polymerization assay was performed following the manufacturer's protocol. The reaction mixture having porcine brain tissue (2 mg/mL) in 80 mM PIPES at pH 6.9, 2.0 mM $MgCl_2$, 0.5 mM EGTA,1.0 mM GTP and glycerol in the presence and absence of test compound **18i** (final concentration of 8 mM) was prepared and added to each well of 96-well plate. Tubulin polymerization was followed by a time dependent increase in fluorescence due to the insertion of a fluorescence reporter into microtubules as polymerization takes place. Spectramax M4 Multi mode Micro plate Detection System was used to measure Fluorescence emission at 440 nm (excitation wavelength is 360 nm). Combretastatin was used as positive control in the assay at 3 μM final concentration. The IC_{50} value was calculated from the drug concentration required for

inhibiting 50% of tubulin assembly compared to control. Another compound namely, Paclitaxel will stabilize the microtubule. The IC_{50} value was calculated from the drug concentration required for inhibiting 50% of tubulin assembly compared to control.

7.2.4. Anti-microtubule effects by immunofluorescence staining

For morphological analysis of nucleus and tubulin network protocol was as follows, A549 cells were seeded on a glass cover slip, incubated for 48 h in the presence or absence of test compounds **18i** and nocodazole at a concentrations of 2 and 4 μM. Cells grown on coverslips were fixed in 4% formaldehyde in phosphate-buffered saline (PBS) pH 7.4 for 10 min at room temperature. Cells were permeabilized for 6 min in PBS containing 0.5% Triton X-100 (Sigma) and 0.05% Tween-20 (Sigma). The permeabilized cells were blocked with 2% BSA (Sigma) in PBS for 1 h. Later, the cells were incubated with the primary antibody for tubulin from Sigma at 1:200 diluted in blocking solution for 4 h at room temperature. Subsequently the antibodies were removed and the cells were washed thrice with PBS. Cells were then incubated with the FITC labeled anti-mouse secondary antibody (1:500) for 1 h at room temperature. Cells were washed thrice with PBS and mounted in medium containing DAPI. Images were captured using confocal microscope (NIKON) [48].

7.2.5. Molecular docking

The molecular docking studies were performed at the colchicine binding site of α,β-tubulin (PDB ID: 1SA0). The coordinates of the crystal structure were obtained from RCSB-Protein Data Bank and suitable corrections were made using Protein Preparation Wizard from the Schrodinger package. Regarding the ligands, molecules were constructed using ChemBio3D Ultra 12.0 and their geometries were optimized using molecular mechanics. The structural comparison of target hybrid with DAMA colchicine-tubulin (1SA0) and nocodazole-tubulin (5CA1) [16] was performed according to the reported protocol using schrodinger. Finally, docking studies were performed according to the standard protocol implemented in Schrodinger software, version 9.9 on the most active molecule. The ligand-protein complex was analyzed for interactions and 3D pose of most active compound **18i** was imaged using Schrödinger.

7.2.6. Cell cycle analysis

A549 cells in 6 well plates were seeded at a density of 1×10^6/ well and were grown overnight in an incubator. The cells were then incubated with 1, 2 and 4 μM concentrations of compound **18i** and after 48 h, collected using 0.25% trypsin-EDTA. The obtained cell pellets were washed and resuspended in PBS. The cells were fixed by pipetting the resuspended cell suspension into 9 mL of 70% ethanol. After 30 min fixation at 4 °C, the ethanol was removed by centrifugation and the cells washed with PBS. After centrifugation, the cells were incubated with propidium iodide staining solution for 15 min in the dark at room temperature. 10,000 cells from each sample analysed for DNA content (propidium iodide fluorescence) using a BD Accuri C6 flow cytometer and subsequent histograms were plotted with using FlowJo™ v10.7.

7.2.7. Wound healing assay (migration assay)

Confluent HUVECs monolayers in 30 mm petri dishes were wounded with 200 μL pipette tips, giving rise to 1 mm wide lanes per well. The cell debris was removed by washing with PBS and cells were supplied with 2 mL of complete medium (controls) or complete medium containing different concentrations compound **18i** (1, 2 and 3 μM). The wounds were observed by phase contrast microscopy immediately and after 30 h incubation.

7.2.8. Colony forming assay

A549 cells in exponential growth phase were seeded into 6-well plates at 4000 cells/well. After 24 h incubation, the culture medium was replaced with medium containing increasing concentrations (1, 2 and 4 μM) of compound **18i** and 1% DMSO (control). The cells were incubated for 7 days and the drug-containing medium was replenished after 3 days. Each treatment was performed in triplicate. After incubation, the cells were washed twice with PBS, fixed with 4% paraformaldehyde for 20 min and stained with crystal violet for a further 15 min.

7.2.9. Nuclear morphological analysis

Changes in the nuclear morphology of A549 cells were determined using Hoechst 33342. In this assay, A549 cells were grown on cover slips in a 6-well plate at a density of 1×10^6 cells/well and were incubated with different concentrations of compounds **18i** for 48 h. The cells were washed with PBS and 4% paraformaldehyde solution was added. The cells were incubated with 2 μg/mL Hoechst 33,242 for 20 min then washed three times with PBS to remove excess dye. The morphological changes in the nuclei were observed using a ZOE™ Fluorescent Cell Imager (BIO-RAD).

7.2.10. Effect on mitochondrial membrane potential

A549 Cells were grown in 24-well plates (5×10^5 cells/mL) and incubated with different concentrations (1, 2 and 4 μM) of compound **18i**. After 48 h incubation, the medium containing the compound was replaced with 500 μL of fresh medium containing 5 μg/mL rhodamine 123 and further incubated for 20 min. The cells were washed three times with PBS to remove excess dye and photographed in red and green channels using a ZOE™ Fluorescent Cell Imager (BIO-RAD).

7.2.11. Effect on intracellular ROS generation

The intracellular ROS levels in A549 cells were determined by carboxy-H_2DCFDA staining. In this assay, A549 cells were incubated with increasing concentrations of compound **18i** (1, 2 and 4 μM) for 48 h. After incubation, the cells were harvested and stained with a 10 μM solution of carboxy-H_2DCFDA in PBS for 20 min at 37 °C. The intensity of the green fluorescence was analyzed using ZOE™ Fluorescent Cell Imager (BIO-RAD).

7.2.12. Quantification of apoptotic cells

A549 cells (1×10^6/well) were grown in 6 well plate and treated with increasing concentrations of compound **18i** for 48 h. After incubation, the cells were trypsinised and washed with PBS. The obtained cell pellet was resuspended in 1x annexin binding buffer. 5 μL of annexin V and 1 μL of PI was added to the resuspended cells and incubated for 15 min at room temp. 10,000 cells from each sample used for analysis using a BD Accuri C6 flow cytometer and the obtained data were analyzed using FlowJo™ v10.7.

Declaration of Competing Interest

The authors declare that they have no known competing financial interests or personal relationships that could have appeared to influence the work reported in this paper.

Acknowledgements

SS and RT are thankful to DoP, Ministry of Chemicals & Fertilizers, Govt. of India, New Delhi, for the award of NIPER fellowship. The authors acknowledge the Micro Nano Research Facility (MNRF), RMIT University, for providing the facilities to carry out cell culture experiments. NIPER-H Research Communication No.: NIPER-H/2020/M091.

Appendix A. Supplementary material

Supplementary data to this article can be found online at https://doi.org/10.1016/j.bioorg.2021.104765.

References

[1] a) N. Moitessier, J. Pottel, E. Therrien, P. Englebienne, Z. Liu, A. Tomberg, C. R. Corbeil, Medicinal chemistry projects requiring imaginative structure based drug design methods, Acc. Chem. Res. 49 (2016) 1646–1657;
b) D. Weigelt, I. Dorange, Lead generation based on compound collection screening, in: J. Holenz, R. Mannhold, H. Kubinyi, G. Folkers (Eds.), Lead Generation: Methods and Strategies, Wiley-VCH Verlag GmbH & Co. KGaA, Weinheim, Germany, 2016, pp. 95–132.c)N. Shankaraiah, A. P. Sakla, K. Laxmikeshav, R. Tokala, Reliability of click chemistry on drug discovery: a personal account, 19 (2019) 1–21.

[2] a) M. Abou-Gharbia, Discovery of innovative small molecule therapeutics, J. Med. Chem. 52 (2009) 2–9;
b) M. Colombo, I. Peretto, Chemical strategies in early drug discovery: an overview of recent trends, Drug Discovery Today 13 (2008) 677–684.

[3] a) L. Costantino, D. Barlocco, Ten years of medicinal chemistry (2005–2014) in the Journal of Medicinal Chemistry: country of contributors, topics, and public-private partnerships, J. Med. Chem. 59 (2016) 7352–7359;
b) I. Aliagas, R. Berger, K. Goldberg, R.T. Nishimura, J. Reilly, P. Richardson, D. Richter, E.C. Sherer, Sustainable practices in medicinal chemistry part 2: green by design, J. Med. Chem. 60 (2017) 5955–5968;
c) G. Wu, T. Zhao, D. Kang, J. Zhang, Y. Song, V. Namasivayam, J. Kongsted, C. Pannecouque, E. De Clercq, V. Poongavanam, X. Liu, P. Zhan, Overview of recent strategic advances in medicinal chemistry, J. Med. Chem. 62 (2019) 9375–9414.

[4] a) D.G. Brown, J. Boström, Where do recent small molecule clinical development candidates come from? J. Med. Chem. 61 (2018) 9442–9468;
b) A.M. Farghaly, O.M. AboulWafa, Y.A.M. Elshaier, W.A. Badawi, H.H. Haridy, H. A.E. Mubarak, Design, synthesis, and antihypertensive activity of new pyrimidine derivatives endowing new pharmacophores, Med. Chem. Res. 28 (2019) 360–379;
c W.-S. Huang, S. Liu, D. Zou, M. Thomas, Y. Wang, T. Zhou, J. Romero, A. Kohlmann, F. Li, J. Qi, L. Cai, T.A. Dwight, Y. Xu, R. Xu, R. Dodd, A. Toms, L. Parillon, X. Lu, R. Anjum, S. Zhang, F. Wang, J. Keats, S.D. Wardwell, Y. Ning, Q. Xu, L.E. Moran, Q.K. Mohemmad, H.G. Jang, T. Clackson, N.I. Narasimhan, V. M. Rivera, X. Zhu, D. Dalgarno, W.C. Shakespeare, Discovery of brigatinib (AP26113), a phosphine oxide-containing, potent, orally active inhibitor of anaplastic lymphoma kinase, J. Med. Chem. 59 (2016) 4948–4964;
d S. Sana, V.G. Reddy, S. Bhandari, T.S. Reddy, R. Tokala, A.P. Sakla, S. K. Bhargava, N. Shankaraiah, Exploration of carbamide derived pyrimidine-thioindole conjugates as potential VEGFR-2 inhibitors with anti-angiogenesis effect, Eur. J. Med. Chem. 200 (2020), 112457.

[5] a) Y. Cao, L. Zheng, D. Wang, X. Liang, F. Gao, X. Zhou, Recent advances in microtubule-stabilizing agents, Eur. J. Med. Chem. 143 (2018) 806–828;
b L. Li, S. Jiang, X. Li, Y. Liu, J. Su, J. Chen, Recent advances in trimethoxyphenyl (TMP) based tubulin inhibitors targeting the colchicine binding site, Eur. J. Med. Chem. 151 (2018) 482–494;
c) L.S. Penna, J.A.P. Henriques, D. Bonatto, Anti-mitotic agents: are they emerging molecules for cancer treatment? Pharmacol. Ther. 173 (2017) 67–82;
d) R. Kaur, G. Kaur, R.K. Gill, R. Soni, J. Bariwal, Recent developments in tubulin polymerization inhibitors: An overview, Eur. J. Med. Chem. 87 (2014) 89–124;
e) J. Seligmann, C. Twelves, Tubulin: an example of targeted chemotherapy, Future Med. Chem. 5 (2013) 339–352.

[6] F. Person, W. Wilczak, C. Hube-Magg, C. Burdelski, C. Möller-Koop, R. Simon, M. Noriega, G. Sauter, S. Steurer, S. Burdak-Rothkamm, F. Jacobsen, Prevalence of βIII-tubulin (TUBβ3) expression in human normal tissues and cancers, Tumour. Biol. 39 (2017), 1010428317712166.

[7] a) F. Naaz, M.R. Haider, S. Shafi, M.S. Yar, Anti-tubulin agents of natural origin: Targeting taxol, vinca, and colchicine binding domains, Eur. J. Med. Chem. 171 (2019) 310–331;
b) Z. Liu, P. Xu, T. Wu, W. Zeng, Microtubule-targeting anticancer agents from marine natural substance, Anti Cancer Agents Med. Chem. 14 (2014) 409–417;
c) C. Dumontet, M.A. Jordan, Microtubule-binding agents: a dynamic field of cancer therapeutics, Nat. Rev. Drug Discov. 9 (2010) 790–803;
d) S. Sana, R. Tokala, D.M. Bajaj, N. Nagesh, K.K. Bokara, G. Kiranmai, U. J. Lakshmi, S. Vadlamani, V. Talla, N. Shankaraiah, Design and synthesis of substituted dihydropyrimidinone derivatives as cytotoxic and tubulin polymerization inhibitors, Bioorg. Chem. 93 (2019), 103317.

[8] a) N.P. Kumar, S. Thatikonda, R. Tokala, S.S. Kumari, U.J. Lakshmi, C. Godugu, N. Shankaraiah, A. Kamal, Sulfamic acid promoted one-pot synthesis of phenanthrene fused-dihydrodibenzo-quinolinones: Anticancer activity, tubulin polymerization inhibition and apoptosis inducing studies, Bioorg. Med. Chem. 26 (2018) 1996–2008;
b) N. Shankaraiah, S. Nekkanti, U.R. Brahma, N.P. Kumar, N. Deshpande, D. Prasanna, K.R. Senwar, U.J. Lakshmi, Synthesis of different heterocycles-linked chalcone conjugates as cytotoxic agents and tubulin polymerization inhibitors, Bioorg. Med. Chem. 25 (2017) 4805–4816;
c) K. Donthiboina, P. Anchi, P.V.S. Ramya, S. Karri, G. Srinivasulu, C. Godugu, N. Shankaraiah, A. Kamal, Synthesis of substituted biphenyl methylene indolinones as apoptosis inducers and tubulin polymerization inhibitors, Bioorg. Chem. 86 (2019) 210–223.

[9] a)S. Nekkanti, O. Ommi, P.S.S. Lakshmi, N. Shankaraiah, Diverse targeted approaches to battle multidrug resistance in cancer, 26 (2019) 7059–7080. b) M. Kavallaris, Microtubules and resistance to tubulin-binding agents, Nat. Rev. Cancer 10 (2010) 194–204;
c) K.E. Arnst, Y. Wang, D.J. Hwang, Y. Xue, T. Costello, D. Hamilton, Q. Chen, J. Yang, F. Park, J.T. Dalton, D.D. Miller, W. Li, A. Potent, Metabolically stable tubulin inhibitor targets the colchicine binding site and overcomes taxane resistance, Cancer Res. 78 (2018) 265–277;
d) E.A. Perez, Microtubule inhibitors: differentiating tubulin-inhibiting agents based on mechanisms of action, clinical activity, and resistance, Mol. Canc. Therapeut. 8 (2009) 2086–2095.

[10] a) V. Lavanya, A.A.M. Adil, N. Ahmed, A.K. Rishi, S. Jamal, Small molecule inhibitors as emerging cancer therapeutics, Integr. Cancer Sci. Therap. 1 (2014) 39–46;
b) N. Khera, S. Rajput, Therapeutic potential of small molecule inhibitors, J. Cell Biochem. 118 (2017) 959–961.

[11] a) E. Vitaku, D.T. Smith, J.T. Njardarson, Analysis of the structural diversity, substitution patterns, and frequency of nitrogen heterocycles among U.S. FDA approved pharmaceuticals, J. Med. Chem. 57 (2014) 10257–10274;
b) K.I. Bhat, A. Kumar, M. Nisar, P. Kumar, Synthesis, pharmacological and biological screening of some novel pyrimidine derivatives, Med. Chem. Res. 23 (2014) 3458–3467;
c) N.C. Desai, G.M. Kotadiya, A.R. Trivedi, Studies on molecular properties prediction, antitubercular and antimicrobial activities of novel quinoline based pyrimidine motifs, Bioorg. Med. Chem. Lett. 24 (2014) 3126–3130.

[12] a) P.C. Diao, W.Y. Lin, X.E. Jian, Y.H. Li, W.W. You, P.L. Zhao, Discovery of novel pyrimidine-based benzothiazole derivatives as potent cyclin-dependent kinase 2 inhibitors with anticancer activity, Eur. J. Med. Chem. 179 (2019) 196–207;
b) C.S. Munikrishnappa, S.B. Puranik, G.V.S. Kumar, Y.R. Prasad, Part-1: Design, synthesis and biological evaluation of novel bromopyrimidine analogs as tyrosine kinase inhibitors, Eur. J. Med. Chem. 119 (2016) 70–82.

[13] a) S. Banerjee, K.E. Arnst, Y. Wang, G. Kumar, S. Deng, L. Yang, G. Li, J. Yang, S. W. White, W. Li, D.D. Miller, Heterocyclic-fused pyrimidines as novel tubulin polymerization inhibitors targeting the colchicine binding site: structural basis and antitumor efficacy, J. Med. Chem. 61 (2018) 1704–1718;
b) F. Xie, H. Zhao, D. Li, H. Chen, H. Quan, X. Shi, L. Lou, Y. Hu, Synthesis and biological evaluation of 2,4,5-substituted pyrimidines as a new class of tubulin polymerization inhibitors, J. Med. Chem. 54 (2011) 3200–3205;
c)K. Donthiboina, P. Anchi, S. Gurram, G. S. Mani, J. Uppu C. Godugu, N. Shankaraiah, A. Kamal, Bioorg. Chem. Doi:10.1016/j.bioorg.2020.104191 (In press). d) C. Jadala, M. Sathish, P. Anchi, R. Tokala, Uppu C. Godugu, V.G. Reddy, N. Shankaraiah, C. Godugu, N. Nagesh, A. Kamal, ChemMedChem. 14 (2019) 2052–2060.

[14] a)G.B. Evans, R.H. Furneax, D.H. Lenz, V.L. Schramm, P.C. Tyler, O.V. Zubkova, Inhibitors of nucleoside phosphorylases and nucleosidases, US20090239885, 2009.
b)R. Bhatt, B. Gong, F. Hong, S.A. Jenkins, J.P. Klein, C.T. Kohm, J. Tulinsky, Pyrimidines and uses thereof, US20090099183, 2009.
c)S. Mahboobi, S, Dove, A. Sellmer, M. Winkler, E. Eichhorn, H. Pongratz, T. Ciossek, T. Baer, T. Maier, T. Beckers, Design of chimeric histone deacetylase- and tyrosine kinase-inhibitors: a series of imatinib hybrids as potent inhibitors of wild-type and mutant bcr-abl, pdgf-rβ, and histone deacetylases, J. Med. Chem. 52 (2009) 2265-2279.

[15] a)S.A. Long, A. Thorarensen, M.E. Schnute, Pyrimidine and pyridine derivatives useful in therapy, WO2013054185, 2013.
b)K. Geng, H. Liu, Z. Song, C. Zhang, M. Zhang, H. Yang, J. Cao, M. Geng, A. Shen, A. Zhang, Design, synthesis and pharmacological evaluation of ALK and Hsp90 dual inhibitors bearing resorcinol and 2,4-diaminopyrimidine motifs. Eur. J. Med. Chem. 152 (2018) 76–86.
c)Pass, M. 2,4,6-Trisubstituted pyrimidines as phosphotidylinositol-3-kinase inhibitors and their use in the treatment of cancer. US20090143384, 2009.

[16] Y. Wang, H. Zhang, B. Gigant, Y. Yu, Y. Wu, X. Chen, Q. Lai, Z. Yang, Q. Chen, J. Yang, Structures of a diverse set of colchicine binding site inhibitors in complex with tubulin provide a rationale for drug discovery, FEBS J. 283 (2016) 102–111.

[17] M. Sisa, D. Pla, M. Altuna, A. Francesch, C. Cuevas, F. Albericio, M. Alvarez, Total synthesis and antiproliferative activity screening of ((±)-aplicyanins a, b and e and related analogues, J. Med. Chem. 52 (2009) 6217–6223.

[18] a) S. Kasibhatla, V. Baichwal, S.X. Cai, B. Roth, I. Skvortsova, S. Skvortsov, P. Lukas, N.M. English, N. Sirisoma, J. Drewe, A. Pervin, B. Tseng, R.O. Carlson, C. M. Pleiman, MPC-6827: a small-molecule inhibitor of microtubule formation that is not a substrate for multidrug resistance pumps, Cancer Res. 67 (2007) 5865–5871;
b) N. Sirisoma, A. Pervin, H. Zhang, S. Jiang, J.A. Willardsen, M.B. Anderson, G. Mather, C.M. Pleiman, S. Kasibhatla, B. Tseng, J. Drewe, S.X. Cai, Discovery of N-(4-methoxyphenyl)-N,2- dimethylquinazolin-4-amine, a potent apoptosis inducer and efficacious anticancer agent with high blood brain barrier penetration, J. Med. Chem. 52 (2009) 2341–2351.

[19] a) M. Salahuddin, A. Shaharyar, Mazumder, Benzimidazoles: A biologically active compounds, Arab. J. Chem. 10 (2017) 157–173;
b) S. Tahlan, S. Kumar, B. Narasimhan, Pharmacological significance of heterocyclic 1H-benzimidazole scaffolds: a review, BMC Chem. 13 (2019) 101.

[20] a) S. Demirayak, U.A. Mohsen, A.C. Karaburun, Synthesis and anticancer and anti-HIV testing of some pyrazino[1,2-a] benzimidazole derivatives, Eur. J. Med. Chem. 37 (2002) 255;
b) A.M. Monforte, S. Ferro, L.D. Luca, G.L. Surdo, F. Morreale, C. Pannecouque, J. Balzarini, A. Chimirri, Design and synthesis of N1-aryl-benzimidazoles 2-substituted as novel HIV-1 non-nucleoside reverse transcriptase inhibitors, Bioorg Med Chem 22 (2014) 1459–1467.

[21] a)A.R. Martyn, H.R. Alan, K. Richard, L. James, S. Andrew, 2,4-Diaminopyrimidine derivatives useful as inhibitors of aurora kinase, WO2009/063240 A1, 2009.
b)S. Turk, B. Merget, S. Eid, S. Fulle, From cancer to pain target by automated selectivity inversion of a clinical candidate. J. Med. Chem. 61 (2018) 4851−4859.
c)C.S. Munikrishnappa, S.B. Puranik, G.V.S. Kumar, Y.R. Prasad, Part-1: Design,

synthesis and biological evaluation of novel bromopyrimidine analogs as tyrosine kinase inhibitors, Eur. J. Med. Chem. 119 (2016) 70–82.

[22] a) J. Zhang, J.L. Wang, Z.M. Zhou, Z.H. Li, W.Z. Xue, D. Xua, L.P. Hao, X.F. Han, F. Fei, T. Liu, A.H. Liang, Design, synthesis and biological activity of 6-substituted carbamoyl benzimidazoles as new nonpeptidic angiotensin II AT1 receptor antagonists, Bioorg. Med. Chem. 20 (2012) 4208–4216;
b) C. Kus, G. Ayhan-Kilcigil, S. Ozbey, F.B. Kaynak, M. Kaya, T. Coban, B. Can-Eke, Synthesis and antioxidant properties of novel N-methyl-1,3,4-thiadiazol-2-amine and 4-methyl-2H-1,2,4-triazole-3(4H)-thione derivatives of benzimidazole class, Bioorg. Med. Chem. 16 (2008) 4294–4303;
c) H.L. Kuo, J.C. Lien, C.H. Chung, C.H. Chang, S.C. Lo, I.C. Tsai, H.C. Peng, S. C. Kuo, T.F. Huang, NP-184[2-(5-methyl-2-furyl) benzimidazole], a novel orally active antithrombotic agent with dual antiplatelet and anticoagulant activities, N. S. Arch Pharmocol. 381 (2010) 495–505.

[23] a) K. Lavrador-Erb, S.B. Ravula, J. Yu, S. Zamani-Kord, W.J. Moree, R.E. Petroski, J. Wen, S. Malany, S.R.J. Hoare, A. Madan, P.D. Crowe, G. Beaton, The discovery and structure–activity relationships of 2-(piperidin-3-yl)-1H-benzimidazoles as selective, CNS penetrating H1-antihistamines for insomnia, Bioorg. Med. Chem. Lett 20 (2010) 2916–2919;
b) K.F. Ansari, C. Lal, Synthesis and evaluation of some new benzimidazole derivatives as potential antimicrobial agents, Eur. J. Med. Chem. 44 (2009) 2294.

[24] a) J. Camacho, A. Barazarte, N. Gamboa, J. Rodrigues, R. Rojas, A. Vaisberg, R. Gilman, J. Charris, Synthesis and biological evaluation of benzimidazole-5-carbohydrazide derivatives as antimalarial, cytotoxic and antitubercular agents, Bioorg. Med. Chem. 19 (2011) 2023–2029;
b) A. Patil, S. Ganguly, S. Surana, Synthesis and antiulcer activity of 2-[5-substituted-1-H-benzo(d) imidazol-2-yl sulfinyl]methyl-3-substituted quinazoline-4-(3H) ones, J. Chem. Sci. 122 (2010) 443–450.

[25] A.D. Ricart, E.A. Ashton, M.M. Cooney, J. Sarantopoulos, J.M. Brell, M.A. Feldman, K.E. Ruby, K. Matsuda, M.S. Munsey, G. Medina, A. Zambito, A.W. Tolcher, S.C. Remick, A phase I study of MN-029 (denibulin), a novel vascular-disrupting agent, in patients with advanced solid tumors. cancer chemotherapy and pharmacology, 68 (2011) 959–970.

[26] S.M. Attia, Molecular cytogenetic evaluation of the mechanism of genotoxic potential of amsacrine and nocodazole in mouse bone marrow cells, J. Appl. Toxicol. 33 (2013) 426–433.

[27] A.E. Prota, F. Danel, F. Bachmann, K. Bargsten, R.M. Buey, J. Pohlmann, S. Reinelt, H. Lane, M.O. Steinmetz, The novel microtubule-destabilizing drug BAL27862 binds to the colchicine site of tubulin with distinct effects on microtubule organization, J. Mol. Biol. 426 (2014) 1848–1860.

[28] a S. Wang, Q. Luo, P. Fan, Cannabisin F from hemp (cannabis sativa) seed suppresses lipopolysaccharide-induced inflammatory responses in BV2 microglia as sirt1 modulator, Int. J. Mol. Sci. 20 (2019) 507;
b Q. Luo, X. Yan, L. Bobrovskaya, M. Ji 1, H. Yuan, H. Lou, P. Fan, Anti-neuroinflammatory effects of grossamide from hemp seed via suppression of TLR-4-mediated NF-κB signaling pathways in lipopolysaccharide-stimulated BV2 microglia cells, Mol. Cell Biochem. 428 (2017) 129–137.

[29] a)P. De, M. Baltas, F. Bedos-Belval, Cinnamic acid derivatives as anticancer agents-a review, Curr. Med. Chem. 18 (2011) 1672–1703.
b)S.M.A. Kamal, N. Nagesh, N. Shankaraiah, S.C. Dushantrao, N.H. Krishna, N-((1-phenyl-9H-pyrido[3,4-b]indol-3-yl)methyl)cinnamamides as Anticancer Agents and Preparation Thereof, WO2017125952A1, 2016.
c)Z. Yuan, Q. Sun, D. Li, S. Miao, S. Chen, L. Song, C. Gao, Y. Chen, C. Tan, Y. Jiang, Design, synthesis and anticancer potential of NSC-319745 hydroxamic acid derivatives as DNMT and HDAC inhibitors, Eur. J. Med. Chem. 134 (2017) 281–292.

[30] a K.N. Patel, V.N. Telvekar, Design, synthesis and antitubercular evaluation of novel series of N-[4-(piperazin-1-yl)phenyl]cinnamamide derivatives, Eur. J. Med. Chem. 75 (2014) 43–56;
b P. Phuwapraisirisan, T. Puksasook, J. Jong-aramruang, U. Kokpol, Phenylethyl cinnamides: a new series of a-glucosidase inhibitors from the leaves of Aegle marmelos, Bioorg. Med. Chem. Lett. 18 (2008) 4956–4958;
c B. Narasimhan, D. Belsare, D. Pharande, V. Mourya, A. Dhake, Esters, amides and substituted derivatives of cinnamic acid: synthesis, antimicrobial activity and QSAR investigations, Eur. J. Med. Chem. 39 (2004) 827–834.

[31] a Z. Wang, D. Xie, X. Gan, S. Zeng, A. Zhang, L. Yin, B. Song, L. Jin, D. Hu, Synthesis, antiviral activity, and molecular docking study of trans-ferulic acid derivatives containing acylhydrazone moiety, Bioorg. Med. Chem. Lett 27 (2017) 4096–4100;
b E.M. Doherty, C. Fotsch, Y. Bo, P.P. Chakrabarti, N. Chen, N. Gavva, N. Han, M. G. Kelly, J. Kincaid, L. Klionsky, Q. Liu, V.I. Ognyanov, R. Tamir, X. Wang, J. Zhu, M.H. Norman, J.J.S. Treanor, Discovery of potent, orally available vanilloid receptor-1 antagonists. Structure-Activity relationship of N-aryl cinnamides, J. Med. Chem. 48 (2005) 71–90;
c B.C. Perez, C. Teixeira, I.S. Albuquerque, J. Gut, P.J. Rosenthal, J.R.B. Gomes, M. Prudencio, P. Gomes, N-cinnamoylated chloroquine analogues as dual stage antimalarial leads, J. Med. Chem. 56 (2013) 556–567.

[32] a B. Nicholson, G.K. Lloyd, B.R. Miller, M.A. Palladino, Y. Kiso, Y. Hayashi, S.T. C. Neuteboom, NPI-2358 is a tubulin depolymerizing agent: in vitro evidence for activity as a tumor vascular-disrupting agent, Anti-Cancer Drugs 17 (2006) 25–31;
b Y. Yamazaki, Y. Kido, K. Hidaka, H. Yasui, Y. Kiso, F. Yakushiji, Y. Hayashi, Tubulin photoaffinity labeling study with a plinabulin chemical probe possessing a biotin tag at the oxazole, Bioorg. Med. Chem. 19 (2011) 595–602.

[33] P.A. Nim, M.S. Joon, R.E. Joo, Y.H. Yun, K.T. Hoon, P.B. Gun, C.Y. Seo, Benzimidazole derivatives as mitochondrial function modulators, US2014/114067 (2014).

[34] B.M. Savall, F. Chavez, K. Tays, P.J. Dunford, J.M. Cowden, M.D. Hack, R.L. Wolin, R.L. Thurmond, J.P. Edwards, Discovery and SAR of 6-Alkyl-2,4-diaminopyrimidines as Histamine H4 Receptor Antagonists, J. Med. Chem. 57 (2014) 2429–2439.

[35] a D. Gerlier, N. Thomasset, Use of MTT colorimetric assay to measure cell activation, J. Immunol. Methods 94 (1986) 57–63;
b V.G. Reddy, T.S. Reddy, S.H. Privér, Y. Bai, S. Mishra, D. Wlodkowic, N. Mirzadeh, S. Bhargava, Synthesis of gold (I) complexes containing cinnamide: in vitro evaluation of anticancer activity in 2d and 3d spheroidal models of melanoma and in vivo angiogenesis, Inorg. Chem. 58 (2019) 5988–5999.

[36] S.B. Hastie, Intercations of colchcine with tubulin, Pharmacol. Ther. 51 (1991) 377–401.

[37] a R.B.G. Ravelli, B. Gigant, P.A. Curmi, I. Jourdain, S. Lachkar, A. Sobel, M. Knossow, Insight into tubulin regulation from a complex with colchicine and a stathmin-like domain, Nature 428 (2004) 198–202;
b O. Bueno, M. Gargantilla, J. Estevez-Gallego, S. Martins, J.F. Díaz, M. Camarasa, S. Liekens, M. Perez-Perez, E. Priego, Diphenyl ether derivatives occupy the expanded binding site of cyclohexanedione compounds at the colchicine site in tubulin by movement of the αT5 loop, Eur. J. Med. Chem. 171 (2019) 195–208.

[38] C.A. Lipinski, Lead- and drug-like compounds: the rule-of-five revolution, Drug Discov. Today Technol. 1 (2004) 337–341.

[39] N. Chandna, K.M. Kumari, C. Sharma, M. Vijjulatha, J.K. Kapoor, P.K. Sharma, QM/MM docking strategy and Prime/MM-GBSA calculation of celecoxib analogues as *N*-myristoyl transferase inhibitors, Virol-mycol 4 (2015) 141.

[40] J.A. Choi, J.Y. Kim, J.Y. Lee, C.M. Kang, H.J. Kwon, Y.D. Yoo, T.W. Kim, Y.S. Lee, S.J. Lee, Induction of cell cycle arrest and apoptosis in human breast cancer cells by quercetin, Int. J. Oncol. 19 (2001) 837–844.

[41] a L.G. Rodriguez, X. Wu, J.L. Guan, Wound-healing assay, Methods Mol Biol. 294 (2005) 23–29;
b T.S. Reddy, H. Kulhari, V.G. Reddy, V. Bansal, A. Kamal, R. Shukla, Design, synthesis and biological evaluation of 1,3-diphenyl-1H-pyrazole derivatives containing benzimidazole skeleton as potential anticancer and apoptosis inducing agents, Eur. J. Med. Chem. 101 (2015) 790–805;
c D. Das, M.A. Barnes, L.E. Nagy, Anaphylatoxin C5a modulates hepatic stellate cell migration, Fibrogenesis & Tissue Repair 7 (2014) 9.

[42] aH. Rafehi, C. Orlowski, G.T. Georgiadis, K. Ververis, A. El-Osta, T.C. Karagiannis, Clonogenic Assay: Adherent Cells, J. Vis. Exp. 49 (2011) 2573. b T.S. Reddy, H. Kulhari, V.G. Reddy, A.V.S. Rao, V. Bansal, A. Kamal, R. Shukla, Synthesis and biological evaluation of pyrazolo-triazole hybrids as cytotoxic and apoptosis inducing agents, Org. Biomol. Chem. 13 (2015) 10136–10149.

[43] a W. Hu, J.J. Kavanagh, Anticancer therapy targeting the apoptotic pathway, Lancet Oncol. 4 (2003) 721–729;
b C. Jadala, M. Sathish, T.S. Reddy, V.G. Reddy, R. Tokala, S.K. Bhargava, N. Shankaraiaha, N. Nagesh, A. Kamal, Bioorg. Med. Chem. 27 (2019) 3285–3298.

[44] V.G. Reddy, S.R. Bonam, T.S. Reddy, R. Akunuri, V.G.M. Naidu, V.L. Nayak, S. K. Bhargava, H.M.S. Kumar, P. Srihari, A. Kamal, 4β-amidotriazole linked podophyllotoxin congeners: DNA topoisomerase-IIα inhibition and potential anticancer agents for prostate cancer, Eur. J. Med. Chem. 144 (2018) 595–611.

[45] a I. Vermes, C. Haanen, H. Steffens-Nakken, C. Reutellingsperger, A novel assay for apoptosis flow cytometric detection of phosphatidylserine expression on early apoptotic cells using fluorescein labelled annexin V, J. Immunol. Methods 184 (1995) 39–51;
b V.G. Reddy, T.S. Reddy, V.L. Nayak, B. Prasad, A.P. Reddy, A. Ravikumar, S. Taj, A. Kamal, Design, synthesis and biological evaluation of N-((1-benzyl-1H-1,2,3-triazol-4-yl)methyl)-1,3-diphenyl-1H-pyrazole-4-carboxamides as CDK1/Cdc2 inhibitors, Eur. J. Med. Chem. 122 (2016) 164–177.

[46] a F. Petrat, S. Pindiur, M. Kirsch, H.D. Groot, Mitochondrial photochemical drugs do not release toxic amounts of 1O(2) within the mitochondrial matrix space, Arch. Biochem. Biophys. 412 (2003) 207–215.

[47] a J.M. Suski, M. Lebiedzinska, M. Bonora, P. Pinton, J. Duszynski, M. R. Wieckowski, Relation between mitochondrial membrane potential and ROS formation, Methods Mol. Biol. 1782 (2018) 357–381;
b V.G. Reddy, T.S. Reddy, C. Jadala, M.S. Reddy, F. Sultana, R. Akunuri, S. K. Bhargava, D. Wlodkowic, P. Srihari, A. Kamal, Pyrazolo-benzothiazole hybrids: Synthesis, anticancer properties and evaluation of antiangiogenic activity using in vitro VEGFR-2 kinase and in vivo transgenic zebrafish model, Eur. J. Med. Chem. 182 (2019), 111609;
c T.S. Reddy, V.G. Reddy, H. Kulhari, R. Shukla, A. Kamal, V. Bansal, Synthesis of (Z)-1-(1,3-diphenyl-1H-pyrazol-4-yl)-3-(phenylamino)prop-2-en-1-one derivatives as potential anticancer and apoptosis inducing agents, Eur. J. Med. Chem. 117 (2016) 157–166.

[48] I. Khan, K.R. Garikapati, A.B. Shaik, V.K.K. Makani, A. Rahim, Md.A. Shareef, V. G. Reddy, M. Pal-Bhadra, A. Kamal, C.G. Kumar, Design, synthesis and biological evaluation of 1, 4-dihydro indeno[1,2-c] pyrazole linked oxindole analogues as potential anticancer agents targeting tubulin and inducing p53 dependent apoptosis, Eur. J. Med. Chem. 144 (2018) 104–115.